(NASA-CR-153260) ON THE ORIGIN OF THE BANGUI MAGNETIC ANOMALY, CENTRAL AFRICAN EMPIRE (Johns Hopkins Univ.) 63 p HC A04/MF A01 CSCL 08N

N77-25703

Unclas
G3/46 31738

ON THE ORIGIN OF THE BANGUI MAGNETIC ANOMALY CENTRAL AFRICAN EMPIRE

by

Bruce D. Marsh

Department of Earth and Planetary Sciences

The Johns Hopkins University

Baltimore, Maryland 21218

Submitted to the National Aeronautics and Space Administration Center under Grant NSG-5090 to The Johns Hopkins University.

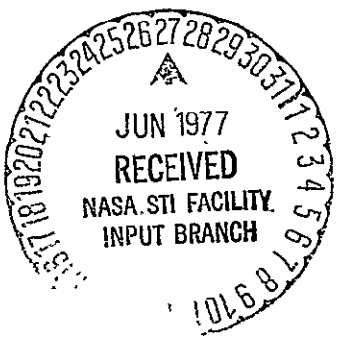

PREFACE

In 1973 Regan, Cain, and Davis recognized a large magnetic anomaly in satellite magnetometer data over the Central African Empire in central Africa. They named this anomaly the Bangui magnetic anomaly due to its location near the capital city of Bangui, C.A.E. Because large crustal magnetic anomalies are uncommon, the origin of this anomaly has provoked some interest and hence this report.

During January of 1976 Regan and I visited the area of the anomaly to make ground magnetic measurements, geologic observations, and in-situ magnetic susceptibility measurements. Some rock samples were also collected and chemically analyzed. Approximately two weeks were spent in the C.A.E. performing field investigations; samples collected during the trip are on file at the Johns Hopkins University and the U. S. Geological Survey.

Our work in the C.A.E. was greatly facilitated by the gracious hospitality bestowed upon us by His Excellency Jean Bedel Bokassa, Emperor for Life of the Central African Empire. Members of his cabinet were also particularly helpful.

The Office de la Recherche Scientifique et Technique Outre Mer (ORSTOM) under the local guidance of Mon. Pierre Morgues was essential in exposing us to the geological and geophysical nature of the C.A.E.; their continual support has made this study possible. J. Vassal and R. Godivier kindly supplied the writer with a preliminary report on the ground magnetic survey. Y. Boulvert most graciously gave the writer a preliminary copy of his new detailed geologic map of the C.A.E. P. Morgues supplied a preliminary version of the Bouguer gravity map of the C.A.E. This report relies heavily on this work and this support is sincerely appreciated.

This work has benefited greatly from numerous discussions and computations with Robert D. Regan. The financial support of the National Aeronautics and Space Administration via the Geophysics Branch has made this study possible.

TABLE OF CONTENTS

PHYSICAL NATURE OF AFRICA

Geology

Africa has been a continent since the early Precambrian. Excepting limited marine transgressions in the Mesozoic Africa has been land since the Ordovician. During much of its early history it was also a land area. Physiographically Africa today is largely a series of flat drainage basins connected by local plateaus, some of which reach an elevation of over 2,000 m. The great East African rift system dominates eastern Africa and the high relief is commonly controlled by near-vertical faulting.

Geologically Africa contains two large cratonic areas, one covering nearly all of south Africa and the other in the nowthwestern part of the continent, many large sedimentary basins, and a significant amount of recent volcanism along the East African Rift and in north-central Africa. Between the large sedimentary basins (Figure 1) are exposures of smaller basins, like the Obangui basin of the Central African Empire (C.A.E.) and their generally granulitic basement rocks.

Seven major orogenic events have been recorded in Africa's rocks.

1. 3000 m.y. ago
2. 2500-2800 m.y.a., Shamvian
3. 1850 ± 250
4. 1100 ± 200 , Kibaran
5. 550 ± 100 , Damaran--Katangan or Pan African
6. mid-Paleozoic--early Mesozoic, Acadian or Hercynian
7. Alpine

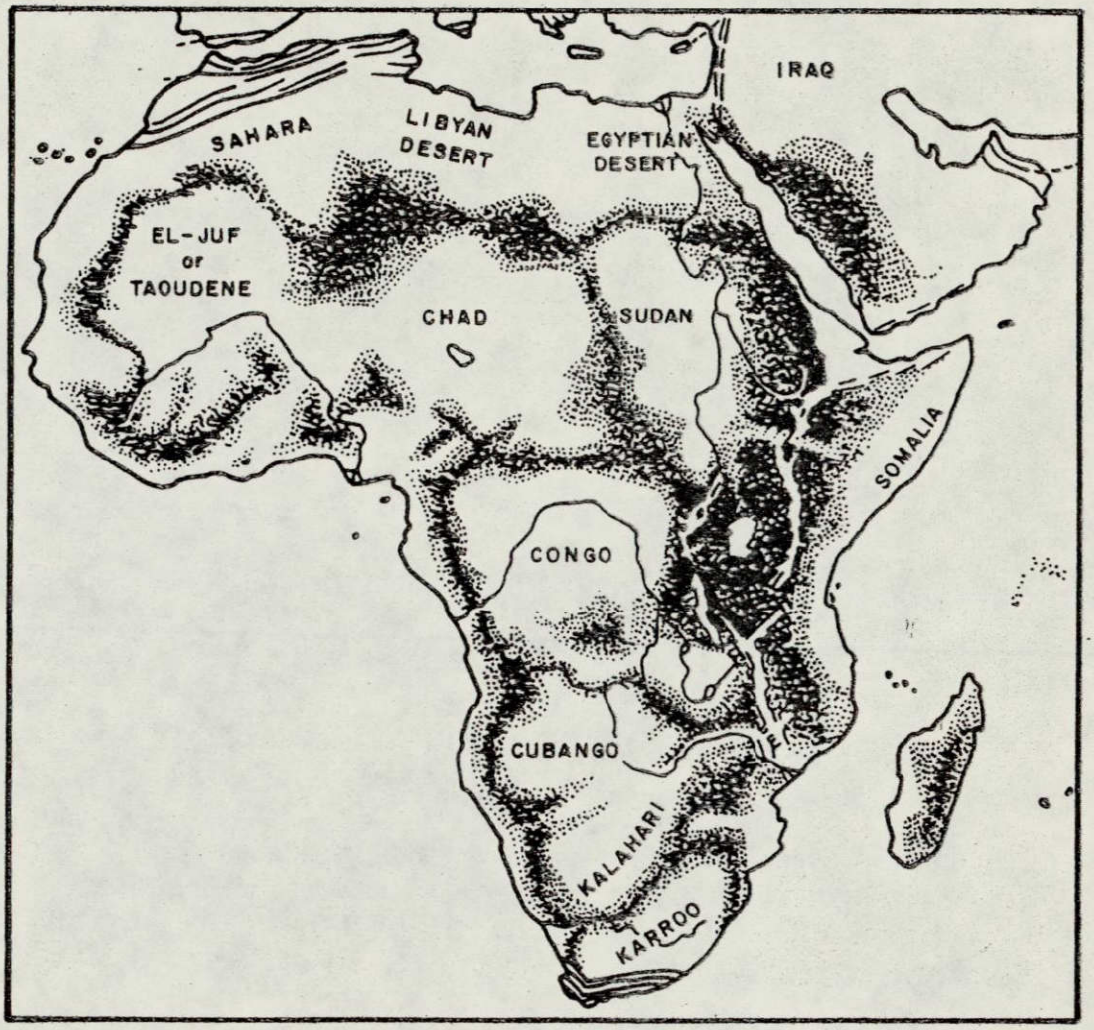

Figure 1. Major basins and tectonic-physiographic provinces of Africa (from Holmes, 1965).

The geographic extent of these events is outlined in Figure 2 from Clifford (1970). The Central African Empire, in concert with most of the continent, suffered extensively from the Kibaran and Pan African events (Cahen and Snelling, 1966). Africa is rather unique in that it contains at least eight nucleii of very old crust (Figure 2). These nucleii, which include, for example, the Barberton Mountain Land of the eastern Transvaal, exhibit rocks and metamorphic events which are 2.5 billion years old or older (Clifford, 1970). Another unique feature of this ancient continent is the Great Dike of Rhodesia, a 480 by about 6 km, northerly trending, ancient (∿2,500 million years), basic intrusive (e.g., Bichan, 1970). The intrusion and extrusion of basic and often ultra basic rocks was not an uncommon event in the early Precambrian of Africa.

Mineral Resources. In general Africa's mineral resources occur in two distinct age-structural units. The younger orogens contain principally copper, lead, zinc, cobalt, beryllium, tin, tungsten, niobium and tantalum. The older cratonic areas contain principally gold, diamonds, chromium, asbestos and iron ore (Clifford, 1966; 1971). The younger orogens are those orogenic events listed already which are younger than about 1100 million years (i.e. 4 to 7 above). The older cratons are those events prior to 1100 m.y. The areas of younger orogens principally border the cratons. And where the craton is nearby, alluvial deposits of craton-like mineral deposits are commonly found. The Central African Empire borders the Congo Basin craton, and it could possess mineral deposits of both types. A substantial iron ore deposit is known as are large alluvial deposits of diamond in the C.A.E. Judging from Clifford's analysis this region may contain other important deposits.

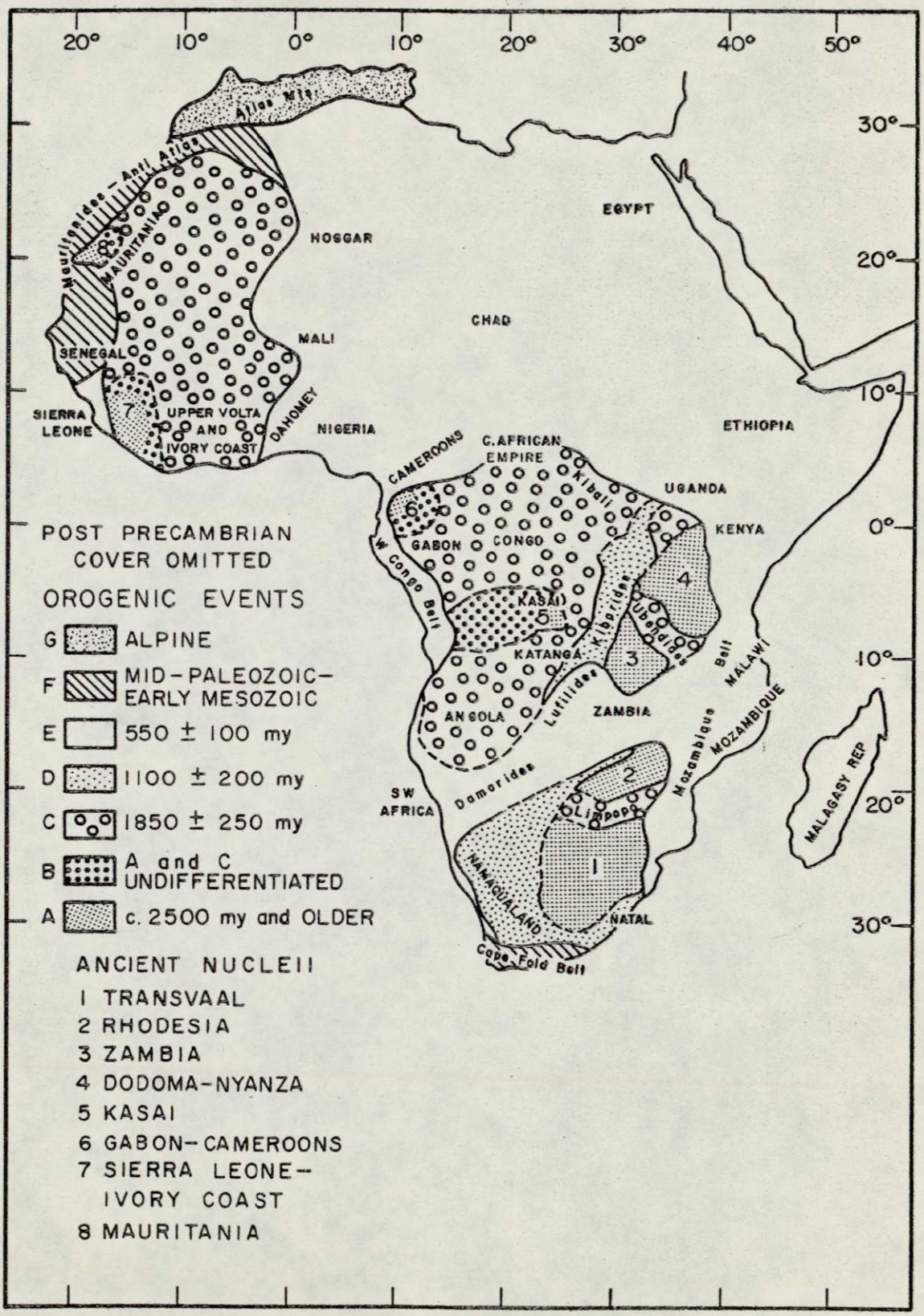

Figure 2. Simplified map of the major structural-orogenic provinces of Africa. (from Clifford, 1970).

To gain a feeling for the importance of various African mineral deposits the following table is given (Clifford, 1971).

African Mineral Production

Mineral	African Production	Percent of World Production (excepting U.S.S.R.)
asbestos	300,000 tons (t)	20
chromite	650,000 t	44
cobalt	11,000 t	73
copper	1,000,000 t	27
diamonds	26,000,000 carats	94
gold	700 t	69
iron ore	9,000,000 t	4
lead	200,000 t	3
tin	19,000 t	13
tungsten (as of 1957)	1,500 t	5
zinc	260,000 t	3

Geophysics

Gravity: A general free-air gravity anomaly map of Africa is shown in Figure 3 (Marsh and Marsh, 1976). The most apparent correlation is between the Congo Basin and the large negative gravity anomaly in this region. The east African Rift system shows as a slight positive, but due to the elevation of this area it will produce a large negative Bouguer anomaly. In general there is not a close correlation between the gravity and the geology.

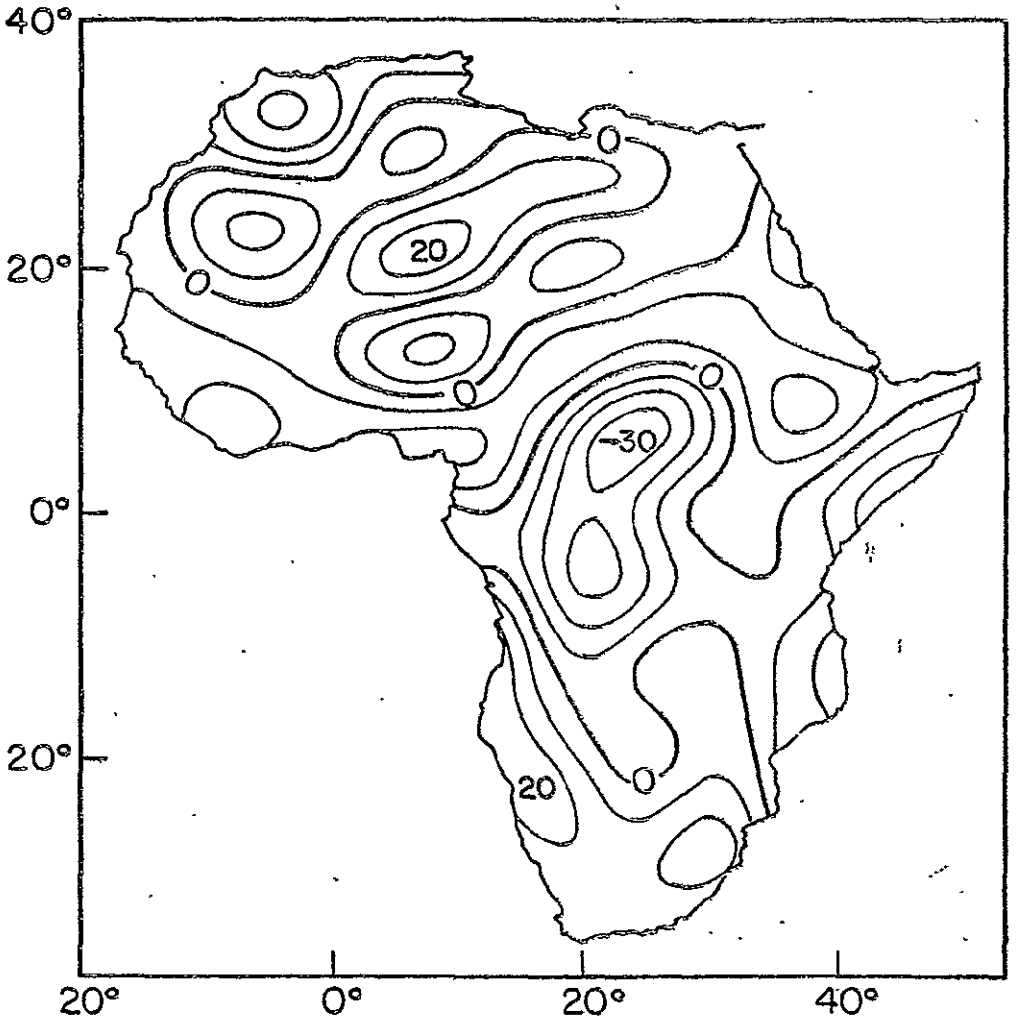

Figure 3. Free air gravity map of Africa based on a combination of satellite and ground measurements (from Marsh and Marsh, 1976); units are mGals.

Magnetics. The satellite total field magnetic anomaly map is shown in Figure 4. (Regan and others, 1975). It was calculated by removing a geomagnetic field model of the 13th degree and order. This anomalous field is not at a constant elevation (∿500-750 km), but at these altitudes the field is slowly varying enough so as to make this variable altitude relatively unimportant. The largest anomaly (∿-10γ) is located over central Africa near the city of Bangui in the Central African Empire (Regan and others, 1973). This anomaly, the Bangui Anomaly, would be a positive if it occurred in northern latitudes; it lies near the geomagnetic equator. Areas of generally positive anomalies are found in the northwestern and southern parts of the continent. These anomalies correlate well with the cratonic shields. And the area of the Congo Basin may similarly be reflected by these anomalies.

Heat Flow. A map of the probable heat flow in Africa is shown in Figure 5 (Chapman and Pollack, 1975; Gass and others, 1977). Although over a good part of Africa there are few heat flow measurements, Chapman and Pollack have used a correlation between geology and heat flow to predict values in areas of no data (1 H.F.U. ∿ 40 mW m^{-2}). Africa shows high heat flows near the East African Rift System and low heat flows in its remaining more tectonically ancient parts. In the interpretation of large crustal magnetic anomalies, like the Bangui Anomaly, it is obviously important to know the limit of magnetization which is largely controlled by temperature.

Crustal temperature can be calculated if the surface heat flow and the magnitude and distribution of heat production is known. The surface heat flow in the C.A.E. is assumed to be that given by Chapman and Pollack.

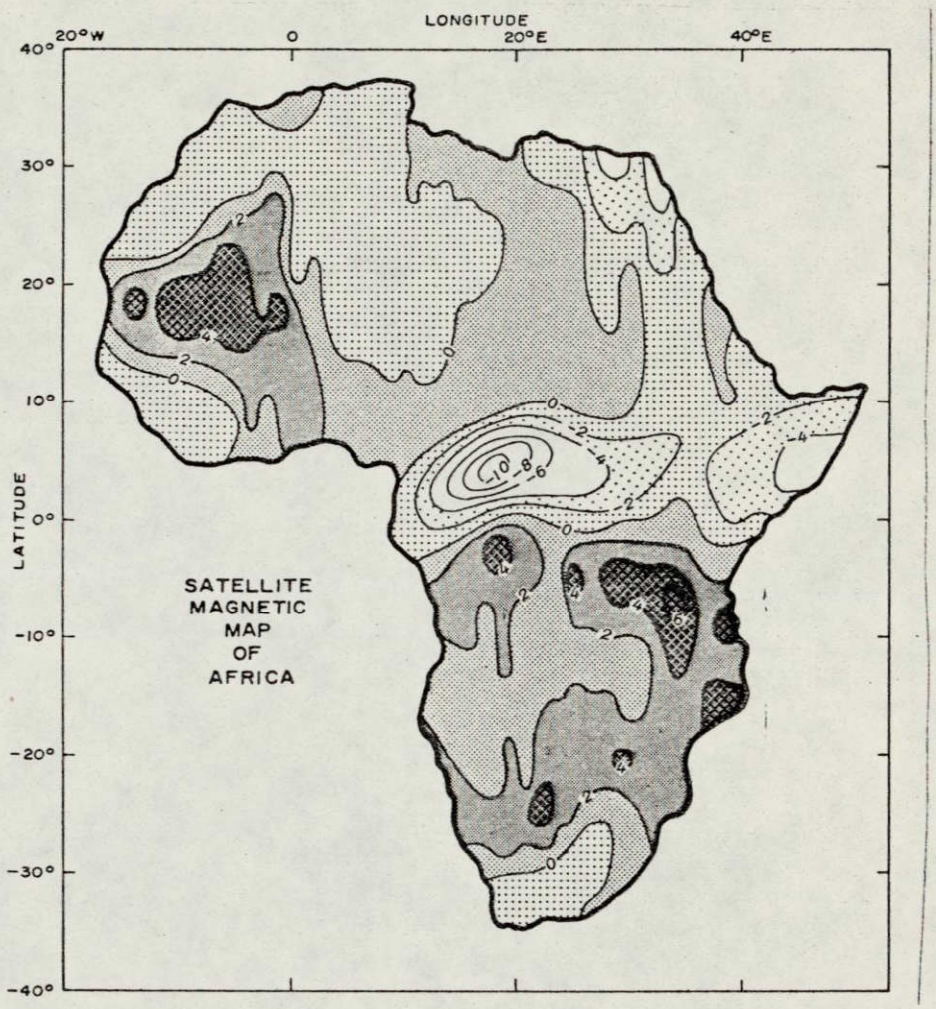

Figure 4. Total field satellite magnetic map of Africa (from Regan et. al, 1975); units are gammas.

The surface heat production can be estimated by assuming the upper crust to be granitic and of Precambrian age whereupon its heat production is about 500 cal km^{-3} s^{-1} or less (e.g. Handbook of Geochemistry). The distribution of crustal heat source is assumed to decay with depth as e^{-BZ}, where B is the reciprocal depth where the surface heat production dies to e^{-1} of its surface value (e.g. Roy, Blackwell, and Decker, 1972).

The steady-state conduction equation describes the crustal geotherm;

$$K_c \frac{d^2T}{dZ^2} = -Ae^{-BZ} \qquad \text{(a)}$$

Where K_c is thermal conductivity, A is heat production, and Z is depth. The boundary conditions are

$$T = 0 \text{ at } Z = 0$$
$$\left(dT/dZ\right)_{Z=0} = q/K_c, \qquad \text{(b)}$$

where q is the surface heat flow. Integrating (a) twice gives

$$K_c T = \frac{-Ae^{-BZ}}{B^2} + C_1 Z + C_2 \qquad \text{(c)}$$

applying (b) to (c) the constants at integration are found to be

$$C_1 = q - A/B$$
$$C_2 = A/B^2 \qquad \text{(d)}$$

Substituting (d) into (c) gives the desired result.

$$T = \frac{A}{K_c B^2}\left(1 - e^{-BZ}\right) + \frac{Z}{K_c}\left(q - A/B\right) \qquad \text{(e)}$$

Figure 5. Regional heat flow in mWatts m^{-2} (40 mW m^{-2} ∿ 1 H.F.U.) from Gass, Pollack and others, 1977.

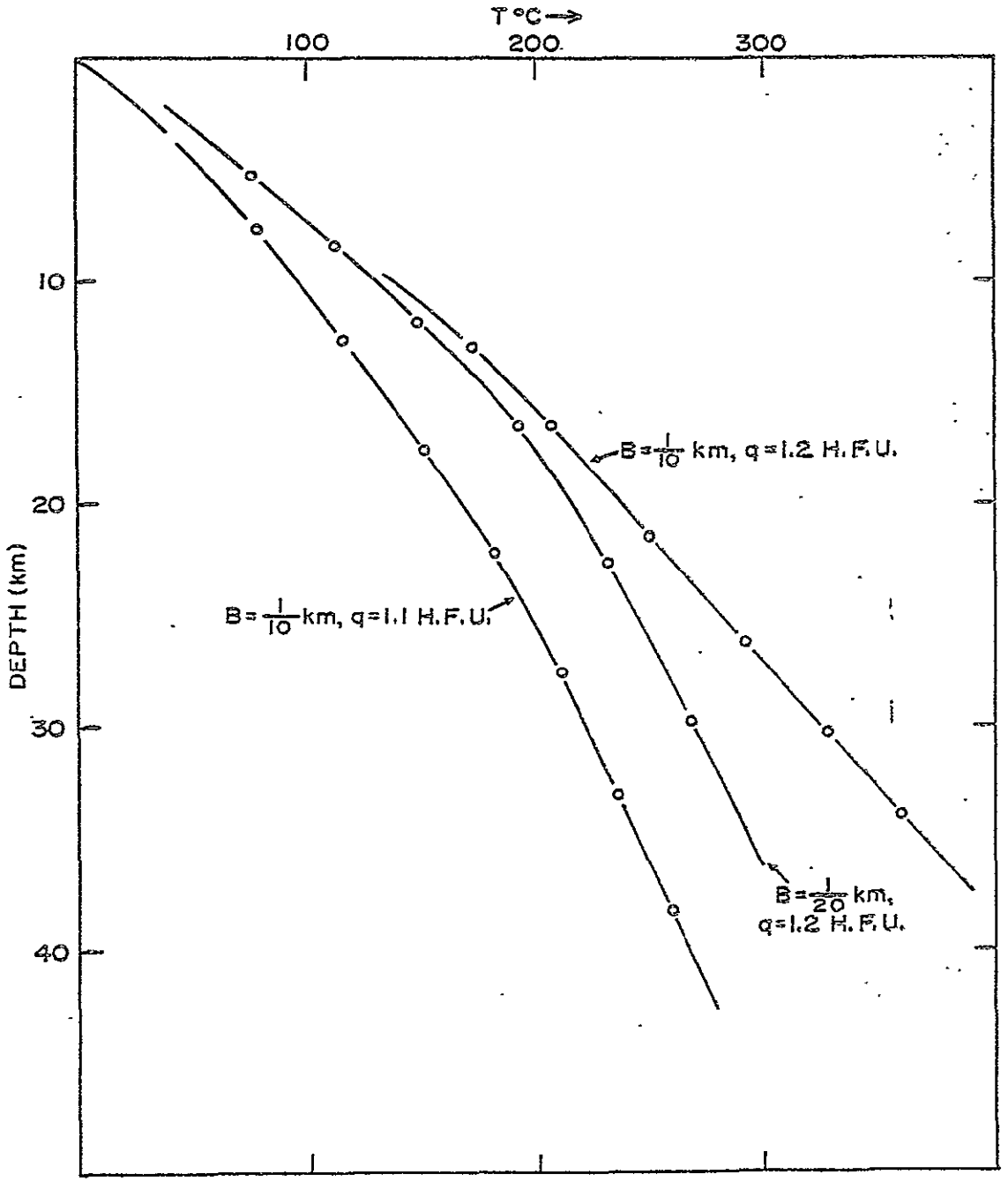

Figure 6. Estimated crustal temperatures beneath the Central African Empire.

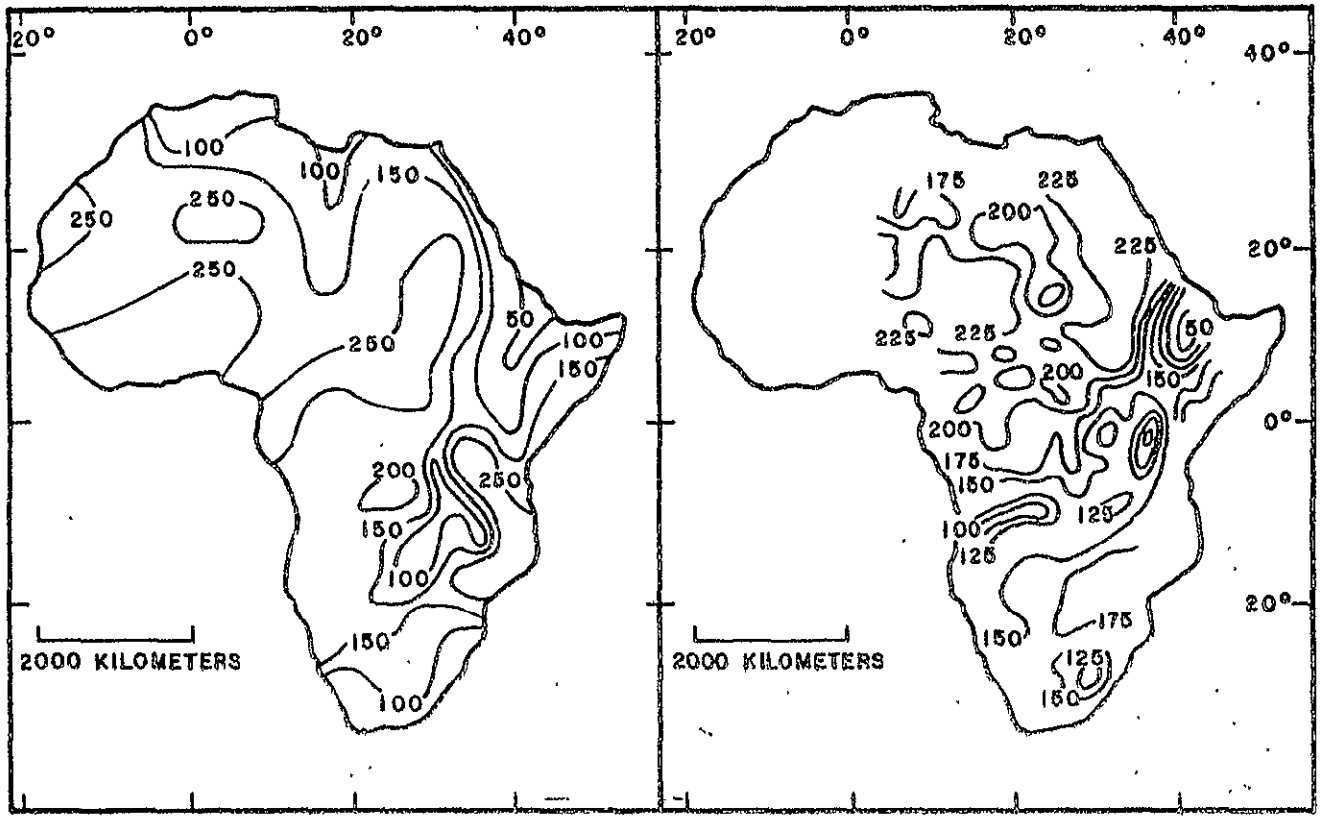

Figure 7. (a) Lithosphere thickness based on heat flow; (b) Lithosphere thickness based on attenuation of surface seismic waves (both from Gass, Pollack and others, 1977).

For A = 500 cal km^{-3} s^{-1} ($\sim$ 2 x 10^{-6} ergs cm^{-3} s^{-1}) and K_c = 3.338 x 10^5 erg cm^{-1} s^{-1} deg^{-1} the curves in Figure 6 were calculated using equation (e). The most realistic curve is probably that where B = 10^{-1} and q = 1.1 H.F.U. in which case the Curie point or limit of ferromagnetism is probably about 40 km, but this depends critically on the exact composition of the magnetite in the lower crust.

A similar calculation can be carried out to determine the depth at which the mantle solidus is exceeded. This has been done by Chapman and Pollack (1977) and this depth gives an estimate of the thickness of the lithosphere. Their map of lithosphere thickness is shown in Figure 7a. As expected, the lithosphere thickness in the tectonically ancient areas of Africa is generally greater than about 200 km.

Seismology. The distribution of larger earthquakes in Africa is shown in Figure 8. They are centered mostly along or near the East African rift system. Although no earthquakes are shown within the C.A.E., some were felt there in 1975 and 1976 (personal communication, P. Morgues, ORSTOM). Because of the paucity of earthquakes and seismograph stations over most of Africa little is known about its crustal structure. Surface wave studies, however, have delineated the general structure and thickness of the lithosphere. This data is reviewed by Gass and others (1977) and Figure 7b which shows lithospheric thickness as adapted from this paper. Lithospheric thickness is defined as the depth to the low-velocity zone or, similarly, the depth where the mantle begins to melt. That is, it is the depth to a critical isotherm. Lithospheric thickness as computed using heat flow and surface heat production (Chapman and Pollack, 1977)

Figure 8. Distribution of earthquake epicenters in Africa (from worldwide map published by U. S. Geological Survey, 1974).

is shown in Figure 7a. These two independent estimates indeed give similar results which attest to the veracity of the predicted values of heat flow over much of Africa.

Summary

African geology is largely dominated by large expanses of stable craton with many large sedimentary basins surrounded by Precambrian rocks of which some form nucleii of some of the oldest rocks on Earth; little has happened tectonically to Africa since the late Precambrian excepting scattered volcanism in the north and widespread volcanism and faulting associated with the extensive East African rift system. The gravity and magnetic fields, for the most part, reflect these features. Surface heat flow does too, and in nontectonic regions the lithosphere is abnormally thick ($\sim$ 200 km) and the Curie point deep ($\sim$ 40 km). Earthquakes are generally confined to the area of the East African rift system. The Central African Empire, containing the Bangui magnetic anomaly, lies between the Congo Basin to the south and the Chad Basin to the north. Its rocks are largely of Precambrian age ($>\sim$ 600 million years) and volcanic activity has been extinct for about 600 million years.

GENERAL GEOLOGY OF THE CENTRAL AFRICAN EMPIRE

INTRODUCTION

The oldest rocks in this area are generally referred to as the basal complex. It, for the most part, is comprised of migmatites, charnokites, metadiabases, and metasediments. Proceeding upwards in the section siliceous sediments become increasingly abundant. These sediments locally form basins which in turn comprise a much larger basin or, perhaps, synclinorium. The basin deposits are intruded by diabase and granitic rocks which have an age of about 550 million years. The principal interest here is in the structural and chemical nature of the above units which can be used to construct a geological and geophysical model to explain the Bangui magnetic anomaly. Thus it is necessary and highly desirable to examine these units and their relations across the C.A.E. in some detail.

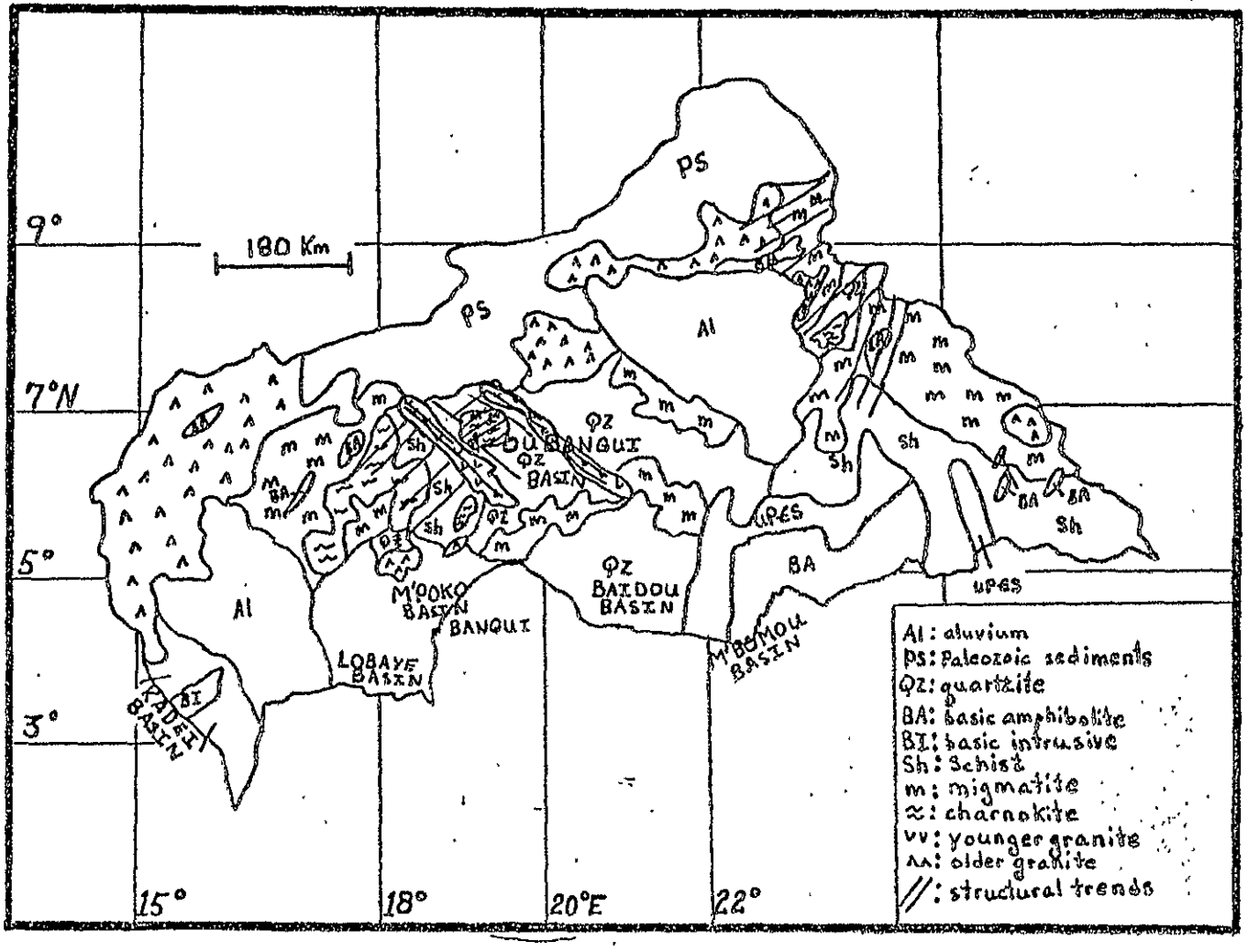

Figure 9a. Generalized geologic map of the Central African Empire (after Mestraud (1953) and Boulvert 1976, personal communication).

BASEMENT

A great deal of work in this region has been carried out by Gerard (1958), Gerard and Gerard (1952; 1954). The rocks most frequently studied belong mostly in the Lower PreCambrian and these are dominantly metasediments. This section rests on the "basal complex" of which this paragraph is concerned. The basal complex has been infrequently studied due to its complexity and poor exposure. In the Baidou basin of West Bangassou the once sedimentary rocks are almost exclusively crystalline schists rich in silica and aluminum with subordinate calc-magnesian (dolomitic) horizons. Often these rocks are found in the granulite facies and as banded biotite-muscovite gneiss. Nearby to the southeast in the M'Bomou basin (Mestraud, 1953) the complex is formed almost completely by metabasalts; the dominant rock type is an anphibole pyroxenite with, garnet, plagioclase, and, oddly enough, quartz. If the appearance of quartz is any indication, these rocks are nearly in the eclogite facies, although the presence of feldspar would indicate possibly a transition from granulite to eclogite. The above area (Baidou basin) borders the magnetic anomaly on the southeast. To the north of the Baidou basin, in the map area of Yalinga-west (see Figure 9) are found a group of highly metamorphosed sediments. Specimens 13 and 14 were collected in this locality (see Figure 9b for sample locations); these show a quartz-rich,

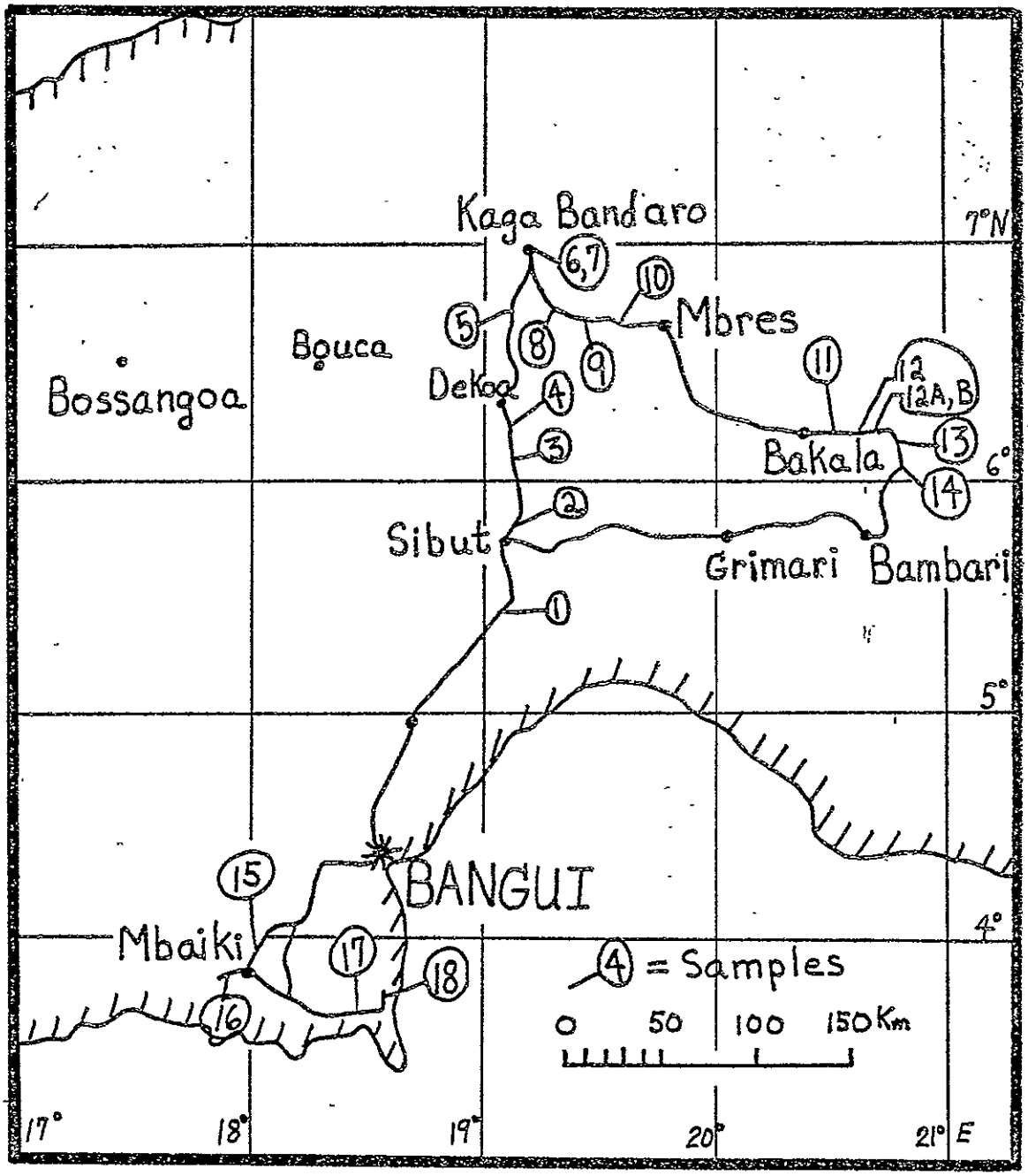

Figure 9b. Locations of samples collected during field trip.

muscovite, biotite, magnetite, and garnet-bearing schist which is in places mylonitic. The trend of the lineations in this area are northeastward with a steep dip to the north. This orientation is typical of the basal complex. In the western part of the C.A.E., Gerard and Gerard (1952) have described a highly metamorphosed sequence of sediments and lavas which are now schists, gneisses, orthogneisses, and migmatites. The orthogneisses include two large masses of charnokite which show little sign of migmatization.

Charnokitic granites near Sibut and Kaga Bandero were inspected on the field trip. One sample (#10) consists of large (~4 mm) clean garnets set in a mass of quartz, plagioclase, and microcline. Magnetite, biotite and xenotine (YPO_4) make up the remainder of the rock. Whole-rock chemical analyses of three so-called charnokites are given below. Sample #10 contains a surprisingly large amount of iron for its silica content.

Sample No.	2	7	10
SiO_2	75.8	75.8	71.5
TiO_2	.14	.17	.65
Al_2O_3	13.6	14.2	13.2
Fe_2O_3	.30	.50	1.5
FeO	1.20	.64	5.9
MnO	.00	.01	.11
MgO	.38	.37	1.4
CaO	.90	1.30	1.0
Na_2O	2.5	2.5	1.4
K_2O	5.7	4.8	3.6
P_2O_5	.04	.04	.08
H_2O+	.50	.53	.40
H_2O-	.11	.18	.10
CO_2	.08	.09	.03

In summary, the basement rocks in the C.A.E. are chiefly made up of highly metamorphosed basic and intermediate composition igneous rocks and siliceous sedimentary rocks.

OUBANGUI BASIN

For our purposes the rocks lying above the basal complex can be divided into the Lower, Upper, and Middle Precambrian. The Lower Precambrian rocks of which the basal complex is a part make up some 75% of the Precambrian exposures. A principal occurance of these rocks is in the central C.A.E. in an area referred to as the Oubangui Basin (Labrousse, 1972). This large sedimentary basin contains a number of smaller or local basins some of which are the Bangoui Kettle, Kotto, Baidou, and M'Bomou basin in the eastern or southeastern part of the Oubangui Basin; the Ombella, Koma, and the Ouaka basin in the central part of the larger basin; and the M'Poko and Lobaye basin in the western part of the Oubangui basin. Judging from the published accounts of the rocks in these smaller basin, and a field trip through the center of the Oubangui Basin the rocks are not sufficently different to warrant separate detailed descriptions, but an overall description of this unit is desirable. The rocks of the M'Poko basin which is north-northwest of the capital city of Bangui has been well documented by Gerard and Gerard (op.cit).

The M'Poko system consists of quartzites, schists, and metavolcanic rocks. The system has been subdivided into three series which previously had two sets of names, one set used in the western Berberati area and another set used in the eastern Berberati area. These two sets have been combined (see Haughton, 1963, p. 29) into the following series (from top (3) to bottom (1))

3. M'Bi and Nola series

2. Pama and Boné series

1. Lin and Kadeï series

The Lin and Kadeï series is the oldest, it rests unconformably upon the basement complex and it is almost wholly made up of light-colored quartzites with small patches of schist.

The Pama and Boné series rests conformably on the above and where the lowest series is absent it rests on the basement complex. This series, unlike the lowest series, is almost entirely schist with small bands of clean quartzite. The schists commonly contain biotite, muscovite, and large garnets.

The youngest M'Bi-Nola series is dominantly fine-grained quartzite in one locality (M'Bi), while the Nola beds are almost exclusively made up of metadiabase of the anphibolite facies. Some tuffaceous schists and quartzites are also present.

The Middle Precambrian rocks of the Lobaye basin lie unconformably upon those of the M'Poko basin. The Lobaye rocks are mostly quartzitic sandstones containing lenses of conglomerate and shale. Numerous outcrops of diabase also occur in this area, and although at first glance they appear intrusive it has been suggested that some may be lava flows. The Lobaye sedimentary rocks are the least metamorphosed of all the sedimentary units visited, although the diabase units are usually intensely chloritized. The diabase obtained by the author from this area contains plagioclase, clinopyroxene, orthopyroxene, magnetite, chlorite, and serpentine. The large pyroxene and magnetite (∿4 mm) form peculiar optically-continuous patches where all perimeters are sure and straight. These minerals are also quite fresh whereas other primary igneous minerals have been largely altered to low temperature equivalents. A chemical analysis of this sample #18 is given below; it is an alkali basalt.

Sample #18 - Alkali Basalt (Diabase)

	(wt%)
SiO_2	47.9
TiO_2	2.1
Al_2O_3	13.8
Fe_2O_3	3.7
FeO	11.2
MnO	.12
MgO	7.4
CaO	7.2
Na_2O	2.0
K_2O	1.2
P_2O_5	.29
H_2O+	2.7
H_2O-	.29
CO_2	.01

Upper Precambrian rocks in the central C.A.E. are principally represented by a series of voluminous and heterogeneous granitic intrusives. A large batholith-like body lies in the area of Sibut and strikes N-NW, and a similar body parallels the Sibut intrusive some 150 km to the east. Both intrusives must cut all the units of the Oubangui basin. These young intrusives largely consist of granite (see analyses below), although it is reported that more basic rocks also occur within these bodies (Pouit, 1959). Thin sections from samples of the intrusive taken by the author near Bembi reveal perthitic microcline, plagioclase, quartz, muscovite, biotite, chlorite, and tiny zircons. It is clear that this rock has been hydrothermally altered under near-surface conditions. A chemical analysis of this sample and some of the heterogeneous granite near Sibut are given below.

Sample	#11	#2 (Pouit)	#3 (Pouit)	#4 (Pouit)
SiO_2	76.1	69.15	46.70	49.80
TiO_2	.09	0.60	1.20	3.07
Al_2O_3	14.0	14.05	15.72	14.02
Fe_2O_3	.59	2.14	3.13	2.92
FeO	.24	2.95	11.59	14.21
MnO	.00	o.27	0.23	0.22
MgO	.15	1.56	7.90	3.15
CaO	.53	2.36	10.62	8.97
Na_2O	3.5	4.66	1.92	2.20
K_2O	5.3	1.54	0.28	0.42
P_2O_5	.04	0.20	0.14	0.49
H_2O+	.11	ignition loss 0.35	0.45	-o.17
H_2O-	.08			
CO_2	.01			
TOTAL		99.83	99.84	99.47

The large intrusive near Bakala shows no sign of deformation or metamorphism. It appears, therefore, as one of the youngest units in the central C.A.E. It is sometimes reported that the intensely metamorphosed banded iron formations (see below) are genetically associated with these bodies, due to their great difference in age this is an unlikely genetic association. Samples 3 and 4 from Pouit (1959, p. 49) contain extraordinary amounts of iron, about 14.7% and 17.1%, respectively. Typical tholeiitic-ocean ridge-basalts and alkali basalts contain about 9 to 11% (wt) total iron. In some areas like Iceland, however, the basalts are commonly more iron rich. Icelandic lavas possessing a silica content similar to analyses 3 and 4 above contain about 11 to 14% (wt) total iron (Carmichael, 1964). If the majority of the iron was held by magnetite, which is indeed likely, the volume percent magnetite could be 3-5% which would imply a magnetic susceptibility of about 10^{-2} (cgs) (Grant and West, 1965, p. 368). Rocks with this susceptibility are uncommon.

Cohen and Snelling (1966) having obtained radiometric ages on a good many of these intrusives and associated units show that most of the ages cluster about 650-500 million years which places them in the Late Precambrian or Early Paleozoic. (See the section on Geochronology for a discussion of these results).

The remaining rocks, some diamondiferous gravels in the extreme western and northeastern parts of the C.A.E. and the Paleozoic sediments of the Chad basin to the north, form only young superficial deposits and hence are of little interest to the explanation of the magnetic anomaly.

BANDED IRON FORMATION

Between Bakala and Ippy (near 6°N, 21°E) a large amount of banded iron formation crops out along the roadside. And at a short distance beyond the road is a large hill (∿ 500m) which consists dominantly of specularite. This unit strikes about N-NW and dips steeply to the east. It seems to be intimately associated with the clean buff to white quartzites so common to the Oubangui Basin. The exact stratigraphic relationship between the iron formation and the quartzite, however, was not established. The hand sample is red with distinct white bands of quartz; the outcrop is laminated on a scale of about 5-10 cm. The iron formation is made up mostly of coarse recrystallized chert grains (∿.8 mm) and finer grains of magnetite and hematite. Limonite and stilpnomelane (?) are also present in trace amounts. The thickness of ore layers of pure quartz grains range from 4 mm to about 1 mm. The ore is usually confined to individual layers having similar thicknesses. The grains of quartz are blocky and the

shape of the magnetite grains is irregular. The rock has been intensely metamorphosed and shows small folds.

James (1955) has shown that the grain size of quartz is a good indicator of metamorphic grade in iron formations. From this criteria this African iron formation represents the highest grade of metamorphism as delineated by James (p. 1475). For a chemical analysis and a general discussion of this formation see the following section on Geology of Economic Interest.

Magnetic Susceptibility Measurements

At each outcrop visited in the C.A.E. the magnetic susceptibility was measured with a Bison Susceptibility bridge possessing an external coil. The coil is about 20 cm in diameter and when placed on the outcrop it samples a spherical area with a diameter of about a meter or so. Due to poor exposure and high degree of weathering fresh surfaces could not be sampled. So these measurements are at best minimum estimates. The charnokitic rocks were highly variable and their susceptibility usually varies in an unpredictable fashion over the outcrop. All the measurements taken are given in the following table.

MEASURED MAGNETIC SUSCEPTIBILITIES

(in c.g.s. units x 10^6)

STOP NO.	AVE.	MAX.	MIN.	NO. OF MEASUREMENTS	ROCK TYPE	CHEMICAL ANALYSIS
1	888	1960	20	6	granite	yes #1
2	661	900	470	12	charnokite	yes #2
3	55	160	0	7	granite	no
4	40	100	10	6	quartzite	no
5	30	70	0	5	quartzite	no
5a	25	55	0	4	mica-schist	no
6	1860	4090	526	10	charnokite	no
7	1587	3270	300	28	charnokite	yes #7
8	27	50	10	3	quartzite	no
9	65	100	50	6	charnokite	no
10	40	70	0	6	charnokite	yes #10
11	35	60	22	16	granite	yes #11
12	8603	23050	2855	7	iron formation	yes #12
13	No measurements - instrument broken					
14						
15	59	85	40	6	diabase	no
16	57	72	49	4	diabase	no
17	59	70	39	4	diabase (weathered)	no
17	471	570	285	4	diabase (semifresh)	no
18	1588	1970	1195	5	diabase (freshest)	yes #18

Geology of Economic Interest

Diamonds

Diamondiferous sedimentary deposits reside in the eastern and western regions of the C. A. E. Heavy mineral separates from these sediments have produced magnesium-rich olivine ($\sim Fo_{90}$) and orthopyroxene ($\sim En_{85}$). These compositions are characteristic of ultramatic nodules of mantle material commonly brought to the surface within kimberlite pipes. Their association with diamond is well-known and characteristic of the important diamond deposits in the Union of South Africa. Even though no kimberlite or diamond pipe has ever been found in the C. A. E. they must surely exist in this general region. The extensive cover of laterite and poor outcrop coverage precludes detailed geologic locationing of such structures. A low-level regional aeromagnetic survey may discover the ultimate sources of the diamonds. There are probably several or more kimbertite pipes which may occur near the margin of the Oubangi basin.

Iron Ore

An apparently substantial deposit of iron ore lies in the region of of Bembi. It is an iron formation of sedimentary origin which is a classic example of the well-known banded-iron-formations (BIF). BIF which occur solely within Precambrian terranes are usually about 2.2 billion

years old (Goldich, 1973: Economic Geology, V. 68, p. 1126-1134). The C. A. E. deposit could also be of this age. Perhaps the most important and well known deposit of BIF occurs in the Lake Superior region of North America. It has been in this region where extensive research has been done on BIF. The BIF of the Lake Superior region has been the principal source of iron ore for the free world (Sims, 1976; Economic Geology, V. 71, pp. 1092-1127).

BIF usually occur as long and narrow trough-like deposits. The exact origin of these deposits remains as one of the most evasive problems in geology. No adequate explanation for their existence has yet been given. The deposits are generally of about 50 to 600 m in thickness and are apparently of both marine and estuarine or fresh water origin. In some areas, for example the Marquette iron range in northern Michigan, the iron formation is intimately associated with tholeiitic volcanic rocks. These basalts are areally extensive and in part represent submarine eruptions. In other areas of BIF the associated formations are marked by a conspicuous absence of any volcanic rocks. This seems to be the case in the Central African Empire. Almost universially BIF are in close association with thick sequences of quartzites. Often these quartzites are so nearly pure SiO_2 that they are of economic interest for making brick and fiberglass. In the C. A. E. a thick white quartzite is associated with the BIF. Although it is not certain, this formation is likely to be of commercial quality.

BIF occur in four principal facies, silicate, oxide, carbonate, and sulphide. A chemical analyses typical of each facies is given in the following table along with an analysis of the C. A. E. iron formation.

Banded Iron Formation Facies

	C. A. E.	Oxide	Carbonate	Silicate	Sulphide
SiO_2	40.9	40.1	26.97	51.18	36.67
TiO_2	.05	-	-	.51	.39
Al_2O_3	1.30	.8	1.30	11.95	6.90
Fe_2O_3	53.3	50.1	2.31	8.09	-
FeO	.84	1.6	39.77	12.15	2.35
MnO	.01	.2	.29	2.71	.002
MgO	.01	2.0	1.99	2.42	.65
CaO	.00	1.4	.66	1.12	.13
Na_2O	.20	-	.09	2.12	.26
K_2O	.02	-		1.86	1.81
P_2O_5	.16	.07	.03	.54	.20
H_2O+	1.7	-	.51	1.19	1.25
H_2O-	.21	-	.10	.07	.55
CO_2	.01	2.6	26.20	3.70	-
	98.8	98.88			

38.7 FeS_2

2.60 SO_3

7.60 C

(analyses from Stanton, 1972; Ore Petrology, McGraw-Hill)

It is clear from these analyses and the petrographic description given earlier in this report that the C. A. E, BIF belong to the oxide or hematite facies. In fact the indiscriminate C. A. E. sample analyzed shows that this formation is indeed of economic grade and it should be further investigated.

Judging from the areal extent of the magnetic anomaly associated with the C. A. E. iron formation the iron formation occupies about 3,000 square km near Bembi. This is of an extent similar to the very important iron ranges in northern Michigan, U.S.A.

STRUCTURAL GEOLOGY

In short, the oldest rocks exhibit a general strike of between about N 20°E and N 40°E while the youngest rocks, the major intrusives, strike nearly perpendicular to the earlier trend. In most instances the oldest rocks are tightly folded and show steep dips.

In the northeastern C.A.E. along the border of Sudan the NE structural trend is obvious from the general geologic map of the C.A.E. (Figure 9). In the north-central Oubangi basin, the quartzites are strongly folded along a roughly north-south axis with near vertical dips.

In the northern most part of Zaire, south of Rafai (5°N, 24°E) in the C.A.E., Cohen (1954, p. 192) has presented a N-S structural profile. He shows the Bondo granite dipping northward under the C.A.E. Above the granite are the basin-filling quartzites and schists with secondary basic intrusives. This structure probably

represents the beginning of the Baidou and M'Bondou basins, however, the occurrance of extensive migmatites and other high grade metamorphic rocks in an east-west band between Grimari and Bambari may indicate the northern limit of these basins and the shallowing of the regional Oubangui basin. North of the Grimari-Bambari migmatite band the quartzites of the presumably M'Poko formation begin again, this marks the beginning of the central Oubangi basin which continues northward for an additional 150 km. The band of migmatites seems surely to have some structural significance for the magnetic anomaly ends abrubtly at this feature.

To the west the Oubangui basin may be terminated by the young heterogeneous granite and the massive charnokites. These latter rocks, which have been described already and are of a high metamorphic grade (granulitic in places), may have once been quite deep seated. Thus they may represent the basement formation of the Oubangui basin - the commonly close proximity of the mica schists which presumably underlies the extensive exposed quartzites may also attests to the shallowing of the Oubangui basin in this region.

In sum, it seems reasonable from the geology that the best preserved and perhaps deepest part of the Oubangui basin-excluding the areas southwest of Bangui - is in the region immediately north of the Grimari-Bambari migmatite band.

GEOCHRONOLOGY

Cahen and Snelling (1966) list 50 radiometric age determinations for the C.A.E.; for completeness these are listed below. Nearly all the determinations were by the Rb-Sr method. The oldest age is 1960 million years and the youngest is 510 million years of which there are two. Most of the ages are in the interval from about 500 to 650 million years which shows the strong effect of the Pan African orogeny in this region. The dated samples belong mostly to the Lower Precambrian and they have been catagorized by Cahen and Snelling into migmatitic and metamorphic basement (group I), heterogeneous metasomatic granites (group II), and intrusive granites (group III). The group to which each specimen belongs is indicated in the table. A map showing the distribution of some of the ages is shown in Figure 10 (Cahen and Snelling, 1966). The young ages of many of the granites which are hardly deformed strongly implies that is was these rocks which were emplaced during the Pan-African orogeny. The large bodies of heterogeneous granites near Sibut and Bakala are surely of this type, and their invasion also probably marks the general time of extensive heating of the crust. This heating probably homogenized much of the crust which now gives young ages.

RADIOMETRIC AGES

No.	Sample	Rock and stratigraphic position	Locality	K:Ar (m.y.)	Rb:Sr (m.y.)
1	Biotite	Gounda granite (II)	Bongo massif, C.A.E.		600±30
2	Biotite	Kaya charnockitic gneiss (I)	Bongo massif, C.A.E.		655±30
3	Biotite	Kaya charnockitic gneiss (I)	Bongo massif, C.A.E.		575±30
4	Biotite	Kaya charnockitic gneiss (I)	Bongo massif, C.A.E.		610±50
5	Biotite	Gneissic enclave (II)	Quango massif, C.A.E.		960±40
6	Biotite	Granite (II)	Quango massif, C.A.E.		885±30
7	Biotite	Quartz-diorite (II)	Zouringi-Grelindji massif, C.A.E.		510±30
8	Biotite	Granite (II)	Zouringi-Grelindji massif, C.A.E.		655±50
9	Biotite	Pegmatite (II	Zouringi-Grelindji massif, C.A.E.		530±30
10	Biotite	Bohobo granite (II)	Bangoran massif, C.A.E.		600±30
11	Biotite	Pegmatite (II), same outcrop as no. 53	Bangoran massif, C.A.E.		610±20
12	Biotite	Gneissic enclave (II), same outcrop as no. 53	Bangoran massif, C.A.E.		590±30
13	Biotite	N'Dele granodiorite (II), same outcrop as no. 53	Bangoran massif, C.A.E.		560±40
14	Biotite	Gneissic enclave (II), same outcrop as no. 53	Bangoran massif, C.A.E.		595±20
15	Biotite	Goussomali granite, heterogeneous facies (II)	Goussomali massif, C.A.E.		515±20
16	Biotite	Gneissic enclave (II), same outcrop as no. 58	Goussomali massif, C.A.E.		635±20
17	Biotite	Pegmatite (II), same outcrop as no. 58	Goussomali massif, C.A.E.		765±30
18	Biotite	Goussomali granite, homogeneous facies (II)	Goussomali massif, C.A.E.		540±10
19	Biotite	Mange granite (II)	Mange massif, C.A.E.		540±20
20	Biotite	Bocaranga homogeneous granite (III)	Bocaranga-Bouar massif, C.A.E.		515±5
21	Biotite	Bocaranga heterogeneous granite (II), same outcrop as no. 63	Bocaranga-Bouar massif. C.A.E.		640±50
22	Biotite	"Lamprophyric" enclave (II), same outcrop as no. 63	Bocaranga-Bouar massif, C.A.E.		615±30
23	Biotite	Migmatite (I)	Bocaranga-Bouar massif, C.A.E.		570±30
24	Biotite	Boukaga homogeneous granite (III)	Bocaranga-Bouar massif, C.A.E.		520±15
25	Biotite	Bouar granite (II)	Bocaranga-Bouar massif C.A.E.		530±10
26	Biotite	Bende gneiss (I)	Bocaranga-Bouar massif, C.A.E.		510±35
27	Biotite	Post-tectonic porphyritic granite (III)	Quandja-Djallé, C.A.E. 8°54'N. 22°48'E.		550±9
28	Biotite	Bohoho (Bohobo) granite (II)	Bohoho or Bohobo, C.A.E. 8°01' N. 20°18'E.		565±11
29	Biotite	Migmatite, Basement Complex (I)	Goboudo Village, C.A.E. 6°26'N. 21°36'E.		580±27
30	Biotite	Gneiss, Basement Complex (I)	Bria ferry, C.A.E. 6°36'N. 22° 00'E.		600±18
31	Biotite	Granitized basement (I)	Quandja-Kotto massif, C.A.E.		610±30
32	Biotite	Gneissic enclave, same outcrop (I)	Quandja-Kotto massif. C.A.E.		610±50
33	Muscovite	Quandja granite (II)	Quandja-Kotto massif. C.A.E.		805±50
34	Biotite	Same granite (II)	Quandja-Kotto massif, C.A.E.		615-15
35	Biotite	Kotto gneiss (I)	Quandja-Kotto massif, C.A.E.		810±40
36	Biotite	Kotto gneiss (I)	Quandja-Kotto massif, C.A.E.		615±50
37	Biotite	N'Daya granite (III)	Djallé massif, C.A.E.		560±30
38	Microcline	N'Daya granite (III)	Djallé massif, C.A.E.		1090±300
39	Microcline	N'Daya granite (III), same as no. 32	Djallé massif, C.A.E.	490±20	
40	Biotite	Djalle granite (III)	Djallé massif, C.A.E.		555±10
41	Microcline	Djalle granite (III)	Djallé massif, C.A.E.		1180±70
42	Biotite	Djalle granite (III), same as no. 34	Djallé massif, C.A.E.	500±20	
43	Biotite	Gneiss (I)	Quijoux massif, C.A.E.		600±10
44	Biotite	Amphibotic enclave (II)	Quijoux massif, C.A.E.		535±30
45	Biotite	Migmatite (I)	Quijoux massif, C.A.E.		570±40
46	Biotite	Migmatite (I)	Quijoux massif, C.A.E.		575±30
47	Biotite	Migmatite (I)	Quijoux massif, C.A.E.		590±50
48	Microcline	Amphibole gneiss (I)	Quijoux massif, C.A.E.		1960±70
49	Microcline	Amphibole gneiss (I), same specimen as no. 38	Quijoux massif C.A.E.	595±20	
50	Biotite	Porphyritic granite (II)	Quandja-Vakaga, C.A.E. 8°54' N 22°48'E		530±7

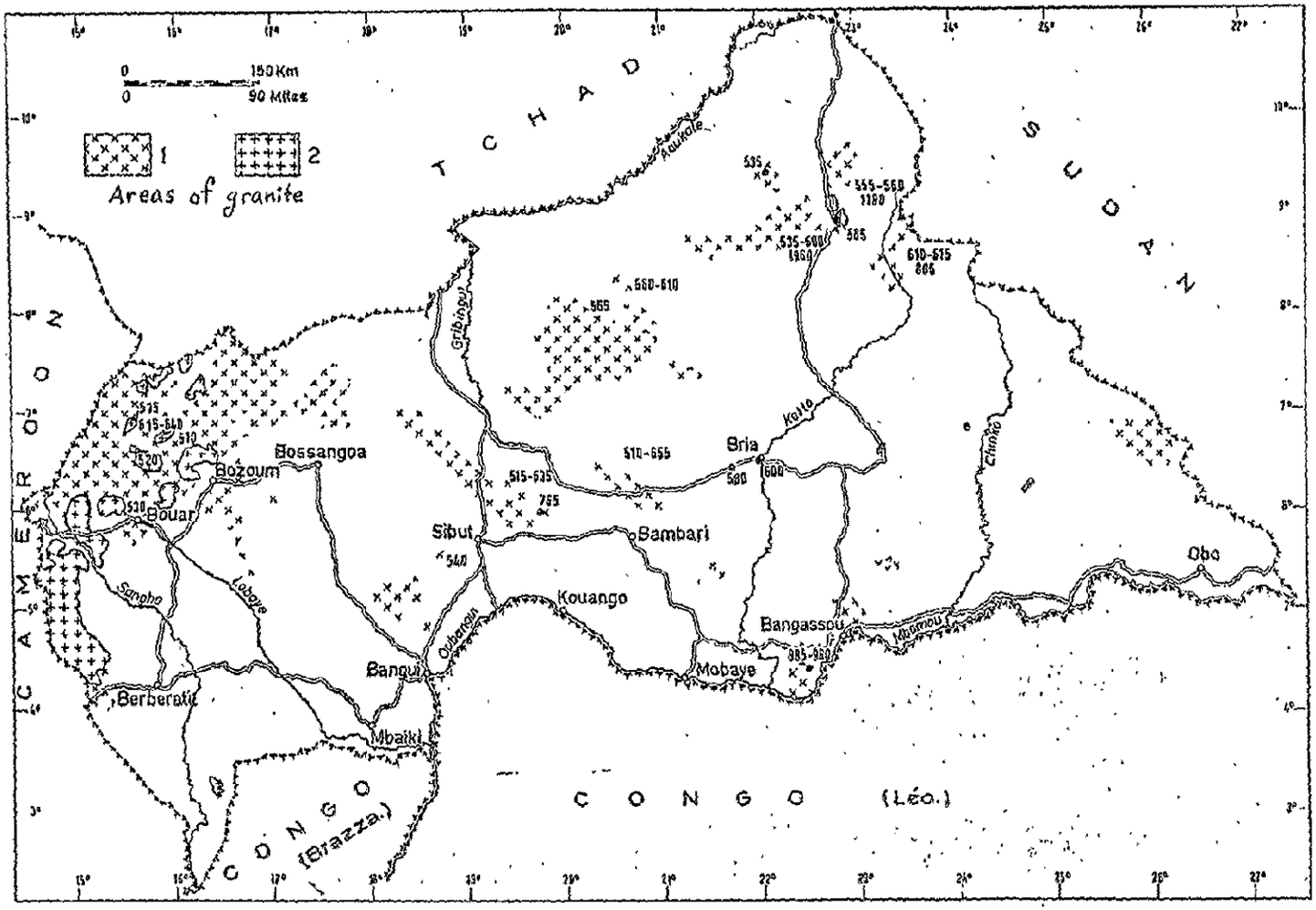

Figure 10. Map showing distribution of age dates on rocks (from Cahen and Snelling, 1966).

TOPOGRAPHY, ISOTASY, AND CRUSTAL THICKNESS

Topography: The land of the C.A.E. is quite flat, its mean elevation is about 550 meters with deviations of $\pm$ 150 m from this datum. The area of main concern, the Oubangui Basin, is a flat basin-like feature with a mean elevation of about 450 m. It is remarkably flat except for an occasional hill of charnokite, quartzite, or granite.

The great age of the crust in this area demands that any isostatic adjustments necessary to achieve hydrostatic equilibrium should have occurred. Even for deformation of a material possessing a yield stress, over long times the rock will deform so as to minimize this yield stress, and the dominant mode of deformation will be by diffusion creep which has all the characteristics of a Newtonian fluid.

Isostasy: If the crust here were of uniform density and isostatic equilibrium prevails, the surface topography should reflect the topography of the Mohorovivic discontinuity. Judging from the distribution of rocks on the surface, it is unlikely, however, that the crust is of uniform density. Hypersthene-bearing granulites show a density range of 2.67 to 3.10 g cm^{-3} with a mean of 2.93 g cm^{-3} (Dobrin, 1976, p. 458). Around the margins of the Oubangui Basin where the massive charnokites (granulites) appear it is likely that the mean density of the crust could be 3.0 to 3.1 g cm^{-3}; this is significantly higher

than the value of 2.67 commonly used as in Bougner correction as the average density of continental crust. Since the quartzites and quartz--mica schists which make up the Oubangui Basin possess a density of about 2.65 and 2.8 g cm^{-3}, respectively, it is possible that mean density of the uppermost part of the crust in this region is less than that where there is no basin. Yet, as will be seen later, a significant negative Bougner gravity anomaly exists in the central C.A.E.

Crustal Thickness: If it could be ascertained that the crust were actually of a uniform thickness over the C.A.E., using the above densities and the condition of isostatic equilibrium a probable density variation within the lower crust might be deduced. Unfortunately there exists almost no seismic data on the crustal thickness in this region of Africa. A value of 41 km is given by Cummings and Shiller (1971) in their global crustal isopach map. Holmes (1965, p. 928) shows a value of about 38 or 39 km for the crustal thickness in a profile through the area of the Congo craton. Without more detailed information on the variation in crustal thickness in Central Africa it is difficult to construct density profiles of the crust. Nevertheless the well-determined Bougner gravity field in the C.A.E. is of great help in determining the variation in crustal density.

GENERAL GEOPHYSICS AND CRUSTAL STRUCTURE OF THE C.A.E.

INTRODUCTION AND SUMMARY

The rocks of the C.A.E. are ancient, little has happened tectonically in this area since the late Precambrian. The crust, then, should be in a state which is close to hydrostatic equilibrium yet a significant negative Bougner gravity anomaly exists over the Oubangui Basin which is correlative with the magnetic anomaly. The crustal thickness is probably within about 5 km of being uniform. The heat flow is probably low at about 40 milliwatts per m^2. The geology outlined already and the observed geophysical features correlate quite closely. These features imply that the Bangui magnetic anomaly can be separated into two parts, a principal part over the Oubangui Basin and a secondary part which has its origin to the southwest of the capital of Bangui. The gravity anomaly and the magnetic anomaly could have a similar source which is principally in the lower one half of the crust. The low heat flow estimates imply temperature low enough to allow rocks at this depth to be magnetic. The formation of the Oubangui Basin and the source of the anomalies can be explained by a basic intrusion into the base of the crust. The following will supply the background information necessary to support these assertions.

MAGNETIC FIELD ANOMALY

The large magnetic anomaly over the Central African Empire shown in Figure 4 was also outlined in the ground-based data of Godiver and Le Donche (1956). This latter survey measured the horizontal and vertical components of the geomagnetic field and declination at 142 locations with the C.A.E. Their anomaly map was acquired by subtraction of a second-order regional field model. If their data is reduced using a 13th degree and order field model, the map shown in Figure 11 is found (Regan 1976). These ground measurements verify the existence of a large magnetic anomaly in this region. The PROGECT magnet aeromagnetic measurements (Stockard, 1971) through this region are shown in Figure 12. Further ground measurements made during the January 1976 field trip to the Oubangui Basin area has enabled the anomaly to be defined even more clearly as shown in Figure 13. These measurements show that the anomaly is comprised of three parts. The principal part centered over the Oubangui Basin and smaller lobes to the northwest and southwest. The 200γ contour (Figure 13) clearly closes about the Oubangui Basin separating the single large anomaly proposed initially into three parts.

The main anomaly over the Basin correlates well with the large negative Bougner gravity anomaly in this region. The anomaly lobes to the southwest and northwest, however, correlate more closely with positive (relative) Bougner gravity anomalies. These gravity anomalies seem to be associated with the band of charnokitic rocks bordering the Oubangui Basin on the west and northwest. The magnetic anomalies here are probably due to the edge effect produced between the sedimentary basin and the charnokitic basement rock. Hence the E-W aeromagnetic profile is probably measuring an edge effect in traversing from the charnokites into the thick section of sediments of the Loboye Basin (Figure 9 and 12).

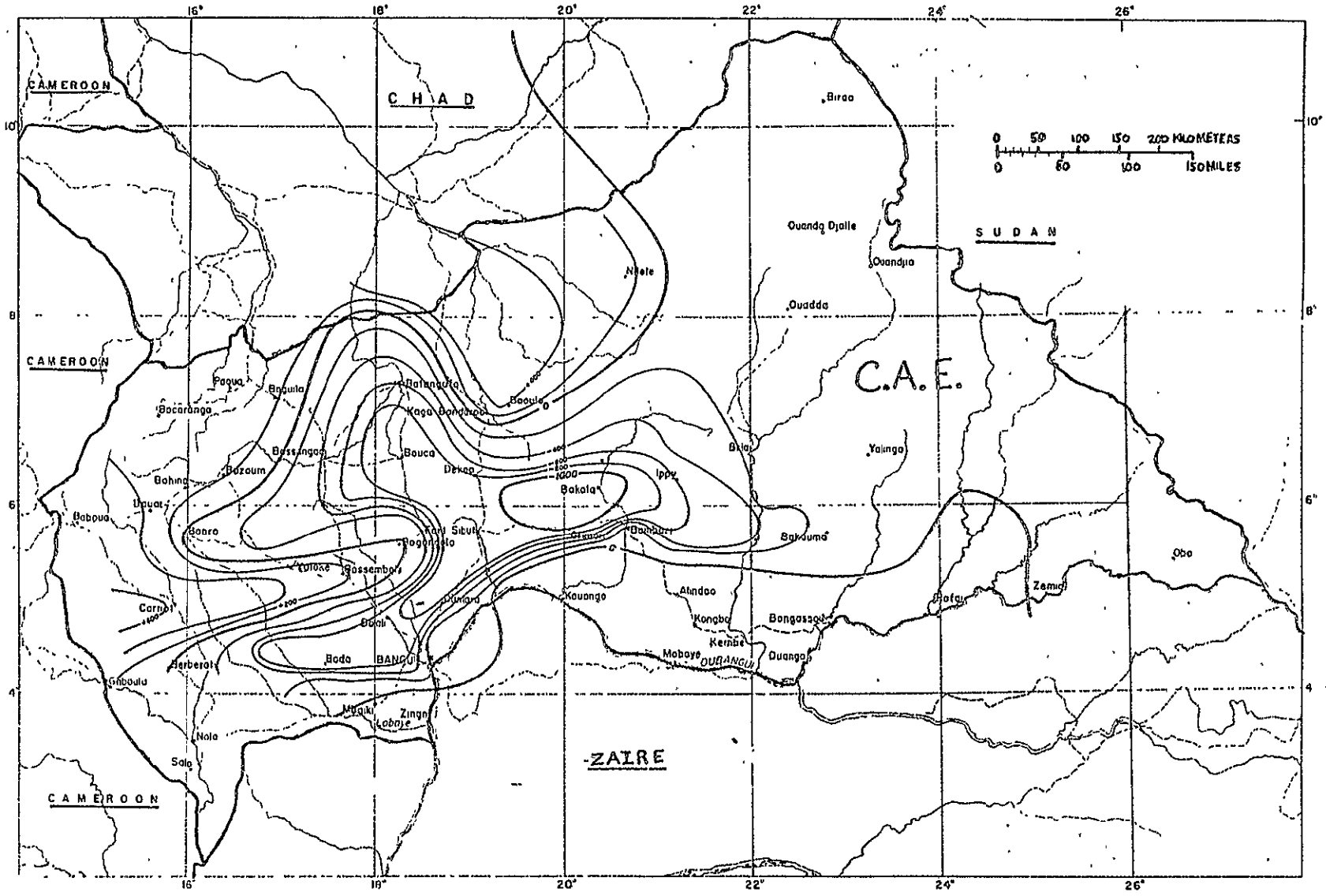

Figure 11. Total field ground magnetic map based on the measurements of Godivier and LeDonche (1956) relative to a 13th degree and order geomagnetic field model (from Regan, 1976).

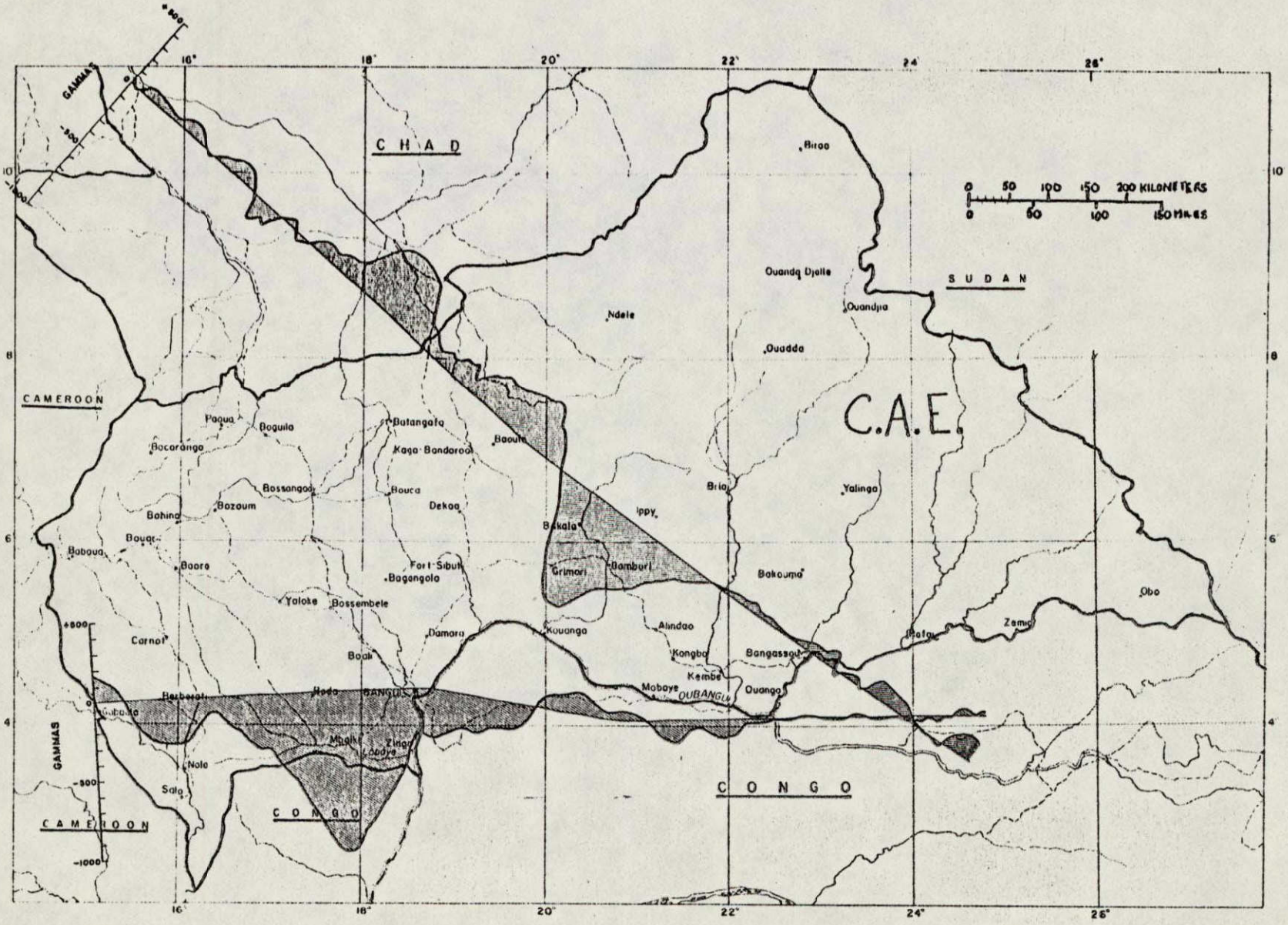

Figure 12. Project MAGNET aeromagnetic traverses over the Central African Empire (from Regan, 1976).

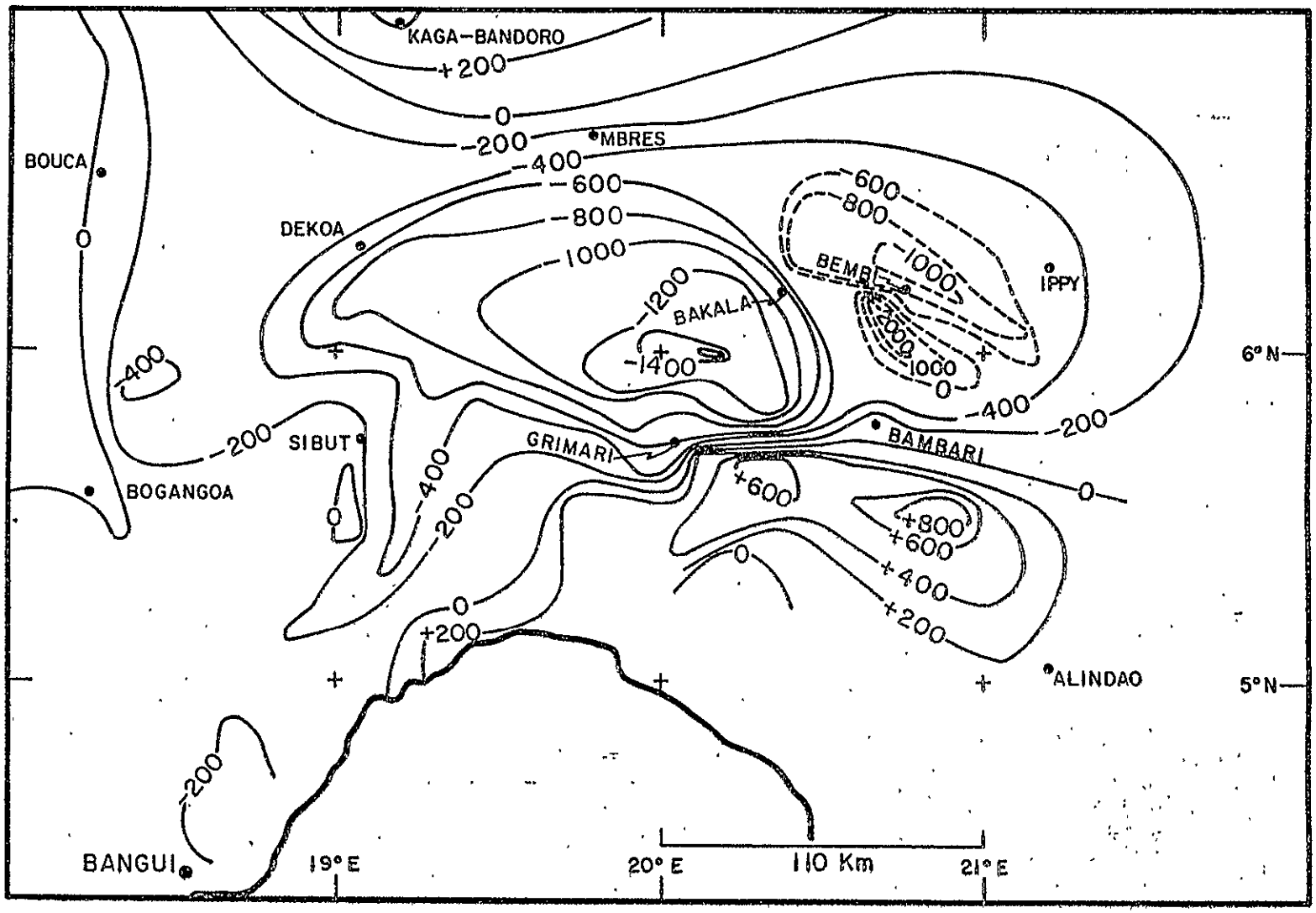

Figure 13. Detailed total field magnetic map based on ground measurements taken by O.R.S.T.O.M. (see Preface) during January 1976 (from O.R.S.T.O.M. personal communication).

BOUGNER GRAVITY FIELD

A Bougner gravity anomaly map of the C.A.E. is shown in Figure 14. The map was supplied by Mon. Morgues of ORSTOM in Bangui, Central African Empire. The map was made from hundreds of observations of the gravitational field mostly along roads with a station spacing of about 2 km. A second-degree regional field was removed from the data by Morgues.

The gravity values are all negative with a range of about 100 m Gals; a typical value is about -70 m Gals. The magnetic anomaly map correlates with the gravity map differently in the two regions of interest. About 100 km west of Bangui the large magnetic low falls near a large positive (relative) gravity anomaly, in the area of the Oubangui Basin the large negative magnetic anomaly falls near the most magnetic part of the Bougner gravity field. These features are shown in Figure 15 which are profiles of the gravitational and magnetic fields along the Project Magnet Flight lines. Other than the distinct low over the Oubangui Basin and the large high (relative) which begins west of Bangui and continues north, fading out for a short distance and wrapping around the north edge of the Oubangui Basin, the map is rather featureless.

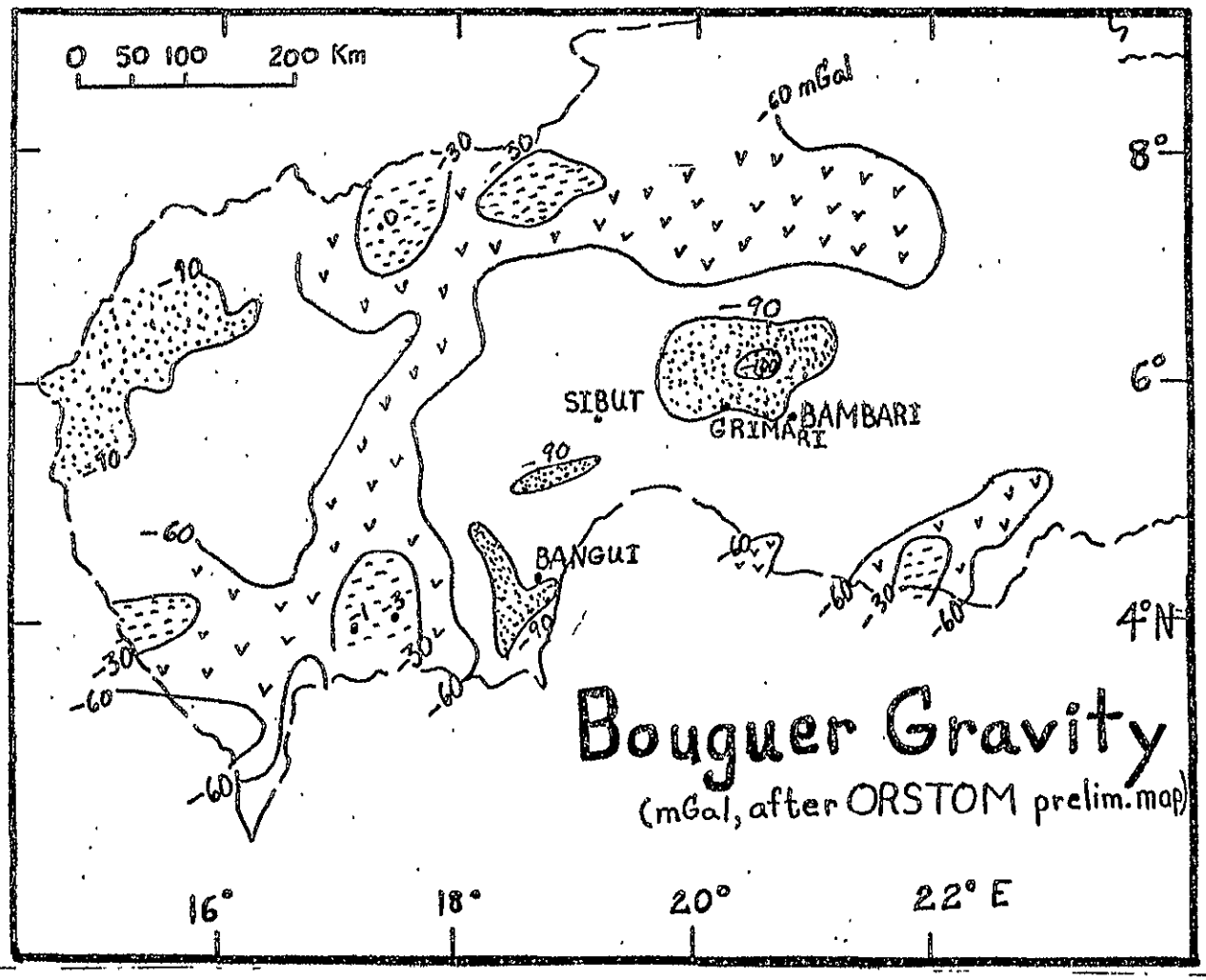

Figure 14. Highly generalized Bouguer gravity map adapted from a detailed map now being compiled by O.R.S.T.O.M. (personal communication P. Morgues (1976)).

A worldwide correlation between crustal thickness and the magnitude of the Bougner anomaly (see Nettleton, 1976, p. 288) indicates for gravity values at -50 to -100 m Gals that the crustal thickness in the C.A.E. should be about 45 to 50 km.

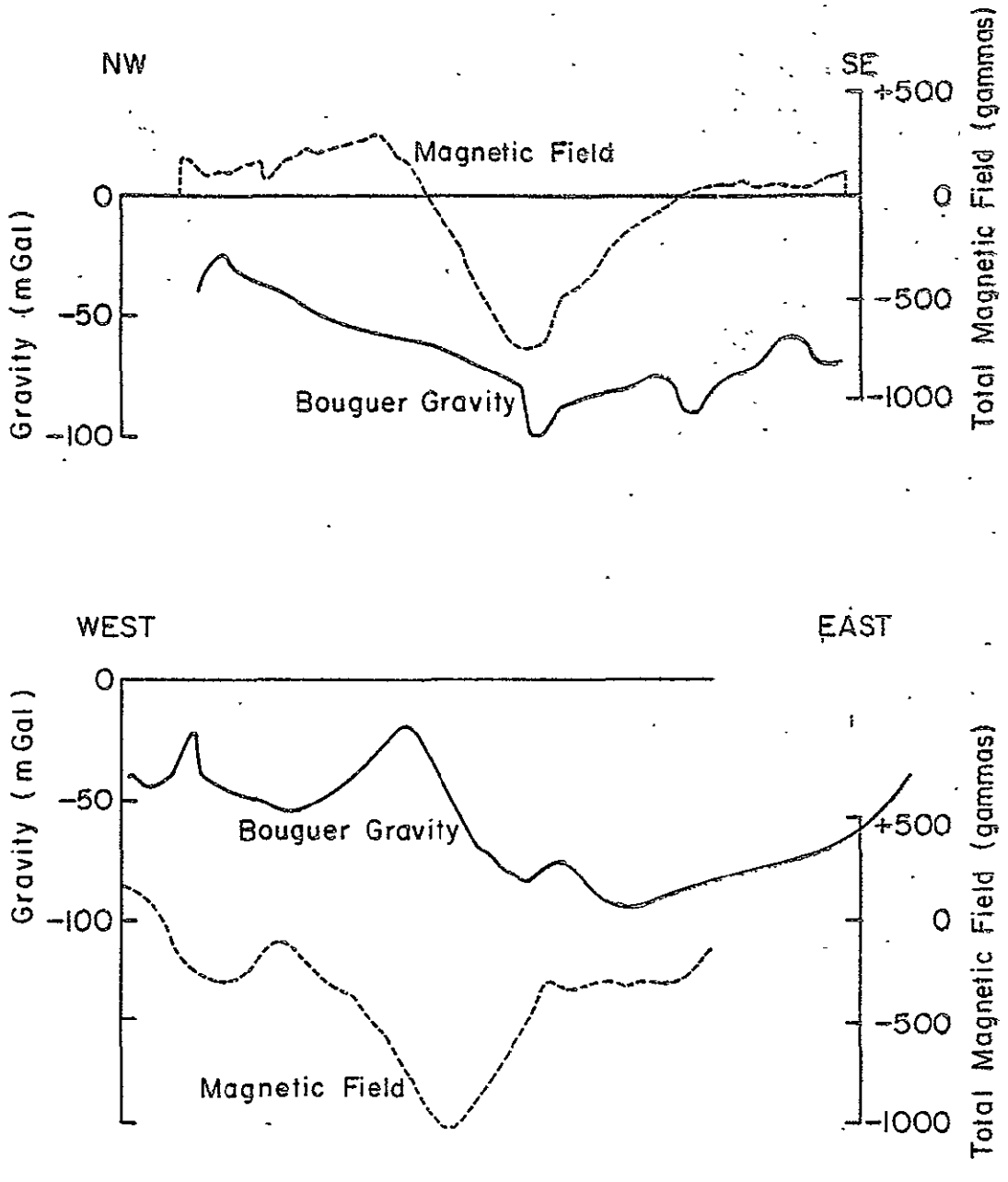

Figure 15. Aeromagnetic (Project MAGNET) and Bouguer gravity profiles along the same lines. Note the correlation of a magnetic low with a gravity low in the top profile, while the lower profile shows a magnetic low near a gravity maximum.

Gross Characteristics of the Anomaly Source

Magnetic Evidence

It is instructive to consider a simple model of the anomaly so as to deduce order of magnitude estimates of its size, bulk intensity of magnetization, and depth. The nearness of the anomaly to the magnetic equator and the roughly circular form of the anomaly suggests a horizontally polarized sphere as an instructive model.

The magnetic attraction of a horizontally polarized dipole can be found from its gravitational potential (ϕ) by use of Poisson's Theorem

$$H_i = \frac{-I}{G\rho} \frac{\partial^2 \phi}{\partial i} \qquad (1)$$

where H_i is the component of the anomaly in the direction i, I is the intensity of magnetization, ρ is density and G is the universal gravitational constant. The gravitational potential is given by

$$\phi = \frac{GM}{r} = \frac{\frac{4}{3}\pi R^3 \rho G}{(x^2 + z^2)^{\frac{1}{2}}} \qquad (2)$$

where R is the radius of the body, ρ is its density, x is the spatial coordinate along the earth's surface measured from the perpendicular bisector from the sphere center, and z is the depth to the center of the body.

$$\frac{\partial^2 \phi}{\partial x^2} = \frac{GM}{z^3} \left[\frac{2\,(x/z)^2 - 1}{((x/z)^2 + 1)^{5/2}} \right] \qquad (3)$$

and evidently

$$H_x = \frac{VI}{z^3} \left[\frac{2(x/z)^2 - 1}{((x/z)^2 + 1)^{5/2}} \right], \qquad (4)$$

where V is the volume of the anomaly-causing sphere. This result gives the horizontal component of the anomaly caused by horizontal induced magnetization. Since $I = \Delta K\, H \cos i$, where ΔK is the difference in apparent magnetic suscepitibility between the body and the country rock, H is the total field strength, and i is the inclination of the inducing field which is zero here, upon substitution (4) becomes

$$H_x = \frac{V\ \Delta K\ H}{z^3} \left[\frac{2(x/z)^2 - 1}{((x/z)^2 + 1)^{5/2}} \right] \qquad (5)$$

Notice that at $x = 0$

$$H_x = \frac{V\ \Delta K\ H}{z^3} = \frac{-4\pi}{3}\ \Delta K\ H\ \left(\frac{R}{z}\right)^3 , \qquad (6)$$

let $R/z = N$ and note that since $N < 1$ (6) becomes

$$\Delta K = -\left(\frac{3}{4\pi}\right)\left(\frac{H_x}{H}\right) \Big/ N^3 \qquad (7)$$

A lower-bound on ΔK is easily found to be ($N < 1$)

$$-\Delta K > \left(\frac{3}{4\pi}\right) \left(\frac{H_x}{H}\right) \qquad (8)$$

Since the total field is nearly horizontal the anomaly amplitude (-1800γ) is approximately H_x and the total field strength (34000γ) is approximately H, then

$$\Delta K > .0126 \qquad (9)$$

where the units are cgs. If N is not unity, but instread the body is say, twice as deep as its radius ΔK > .10. Even the lower estimate given by (9) represents a susceptibility contrast which is much larger than that normally encountered in geophysical exploration and ocean magnetic surveys, but if the body can be brought closer to the surface this lower bound can be reduced. Hence it is worthwhile to consider the less physically imaginable instance of a horizontal dipole of length ℓ and strength m, over the midpoint of the dipole

$$H_x = \frac{-m\ell}{r^3} \qquad (10)$$

where r is the distance from the surface midpoint (x = 0) to the end of the dipole. If d is the depth to the dipole then

$$H_x = -m\ell \left[d^2 + (\ell/2)^2 \right]^{-3/2} \qquad (11)$$

The strength of the dipole is given by m = IV which upon assuming a cylindrical volume for V, becomes $m\ell = \Delta K\ H\cos i\ \pi\ R^2\ \ell$, with i = 0 (11) becomes

$$H_x = \frac{-\Delta K\ H\ \pi\ R^2 \ell}{d^3}\ \left[\ 1+ \left(\frac{\ell}{2d}\right)^2\right]^{-3/2} \qquad (12)$$

Letting R/d = n and $\ell/d = P$ (12) becomes

$$H_x = -\Delta K\ H\ \pi\ P\ n\ \left[\ 1+ \left(\frac{P}{2}\right)^2\right]^{-3/2} \qquad (13)$$

Since n <1 but ℓ is positive but unbounded

$$H_x < -\Delta K\ H\ \pi\ P\ \left[\ 1+ \left(\frac{P}{2}\right)^2\right]^{-3/2} \qquad (14)$$

(14) cannot be further reduced with considering the dimensions of the actual anomaly. The anomaly is about 100 Km long while the depth to the Curie point is probably not greater than about 50 Km, hence $\vec{P} \sim 2$.

$$H_x < -2.22\ \Delta K\ H \qquad (15)$$

or

$$\Delta K > -.45\ \frac{H_x}{H} \qquad (16)$$

Again with $H_x = -1800\gamma$ and $H = 34000\gamma$

$$\Delta K > .0238.$$

If P = 1 then $\Delta K > .0233$, and if P = 3 $\Delta K > .098$; the results are not particularly sensitive to P. In sum, with these simple models of a horizontal polarized sphere and cylinder the anomalous susceptibility must be greater than about .01 (Cgs) to cause an induced anomaly of -1800γ in an inducing field of $34,000\gamma$. This lower bound is, however, seemingly unrealistic from everyday experience.

If the very local maximum of 1800γ measured on the ground is ignored and the amplitude (1000γ) measured aeromagnetically is used in the above calculations, the following results are obtained.

Sphere model: $\Delta K > .007$

Horizontal Dipole model: $\Delta K > .013$

This estimate will probably satisfy the more regional requirements.

Depth to the Body:

A rather simple upper bound on the depth to the center of an anomalously magnetized sphere is apparent from (4) by noting its zeros are given by

$$x/z = \pm\, 2^{-\frac{1}{2}}$$

or the depth is given by

$$z \sim \pm\, 1.4\ x\ . \tag{17}$$

The anomaly is roughly 100 Km across from north to south, x is then 50 Km and the maximum depth to the model body is found 70 km. This estimate is completely dependent on the body being a sphere and proper identification of the outer edge or zeros of the anomaly.

A perhaps more accurate depth estimate comes from considering the variation of the anomaly amplitude with height. At x = 0, (6) gives upon differentiation with respect to z

$$\frac{\partial H_x}{\partial z} = \frac{3\ V\ \Delta K\ H}{z^4} \sim -3\ \frac{H_x}{z}\ . \tag{18}$$

The anomaly amplitude as observed by the Project Magnet profile, which did not actually cross the anomaly at x = 0, is about -1000γ at a height of about 2 km above ground. The anomaly on the ground beneath the project magnet profile has an amplitude of about -1300γ, thus

$$\frac{\partial H_x}{\partial z} \simeq \frac{\Delta H_x}{\Delta z} \simeq \frac{-3H_x}{H} \quad ; \tag{19}$$

and the depth is

$$z \simeq -3\Delta z \left\{\frac{H_x}{\Delta H_x}\right\} \tag{20}$$

with $\Delta z \simeq 2$ km, and $\Delta H_x \simeq 300\gamma$. The depth is

$$z \simeq 26 \text{ km} \tag{21}$$

This result being much more sensitive than the previous estimate (17) can be regarded as quite accurate.

Size of the Body:

A rather simple means to estimate the volume of the anomalous body is to assume a model and estimate its dipole moment. From the dipole moment can be recovered a probable volume. Equation (10) gives the dipole moment as

$$M = m\ell = -r^3 H_x \tag{22}$$

which for a dipole depth of 30 Km and a length of 100 Km and $H_x = -1800\gamma$,

$$M = 3.6 \times 10^{18}, \text{ c.g.s.} \tag{23}$$

Noting that $M = \Delta K \text{ Vol. } H$, where ΔK is the susceptibility difference, Vol. is the body volume, and H is the total field strength (.34 oe), from (23)

$$\text{Vol.} = \frac{1.06 \times 10^{19}}{\Delta K} \tag{24}$$

Inserting the previously derived estimates of $\Delta K \sim .015$, (24) gives the anomalous volume as,

$$\text{Vol.} \underline{\sim} 7 \times 10^{20} \text{ cm}^3 \tag{25}$$

or

$$\text{Vol.} \underline{\sim} 7 \times 10^{5} \text{ Km}^3$$

To gain some feeling for this volume estimate, picture a disk of thickness 50 Km and radius of 67 Km which has an equivalent volume. The volume of anomalously magnetic rock needed to satisfy the anomaly is not small. The spherical model gives a similar result since it too is essentially a dipole.

Gravity Evidence:

The large negative Bouguer gravity anomaly which appears in the area of the magnetic anomaly can also be used to estimate the mass deficiency associated with the anomaly. Considering their close correlation it seems reasonable to expect a similar cause for each. In the gravity case, however, only the volume of the mass deficiency can be determined with any certainty.

Poisson's equation

$$\nabla^2 \phi = 4\pi\rho G = \vec{\nabla} \cdot \vec{g} \tag{26}$$

can be integrated using Gauss' Theorem in the form

$$\int_s \vec{A} \cdot d\vec{s} = \int_v \vec{\nabla} \cdot \vec{A}\, dv \tag{27}$$

Where A is any vector field. In the present instance we replace A by g in (27) to obtain

$$\int_s \vec{g} \cdot d\vec{s} = \int_v \vec{\nabla} \cdot \vec{g}\, dv \tag{28}$$

but using Poisson's equation (26)

$$\int_v \vec{\nabla} \cdot \vec{g}\, dv = \int_v 4\pi\rho G\, dv \tag{29}$$

or finally

$$\int \vec{g} \cdot d\vec{s} = 4\pi G \int \Delta\rho\, dv \tag{30}$$

where now ρ has been replaced by the more appropriate anomalous density $\Delta\rho$. The above relation states that if the component of $\vec{g}$ normal to a surface S which encloses the anomalous mass is integrated over S the result will give the mass deficiency or excess which is represented by the integral on the right in (30). This relation can be further reduced by imagining S to be a spherical surface enclosing the anomalous mass M and by breaking this sphere into an upper (top) and lower (lower) hemisphere.

$$\int_s \vec{g} \cdot d\vec{s} = \int_{top} \vec{g} \cdot d\vec{s} + \int_{lower} \vec{g} \cdot d\vec{s} = 4\pi GM \tag{31}$$

If the radius (R) of the lower hemispherical surface is allowed to get very large then g will be sufficiently normal to S everywhere whence

$$\int_{\text{lower}} \vec{g} \cdot d\vec{s} = \int_{L} \vec{g} \cdot \hat{n}\, dA = \int_{L} |\vec{g}||\hat{n}|\cos\theta dA = \int_{L} |\vec{g}| dA \qquad (32)$$

where n is a unit normal to S and dA is a differential surface area. But furthermore

$$|g| = \frac{|F|}{m} = \frac{GM}{R^2} \qquad (33)$$

Putting (33) into (32) gives

$$\int_{L} \vec{g} \cdot d\vec{s} = \frac{GM}{R^2} \int_{L} dA = \frac{GM}{R^2} 2\pi R^2 = GM\, 2\pi$$

then (31) becomes

$$\int_{\text{Top}} \vec{g} \cdot d\vec{s} = 2\pi GM \qquad (34)$$

which is the desired result. To evaluate (34) the surface S, which is arbitrary, is chosen to be the earth's surface and, since the measured gravity component is nearly normal everywhere to the earth's surface, the volume under the two-dimensional plot of gravity versus distance gives(34).

/ In the Bangui region the anomaly can be adequately approximated by a hemispherical ellipsoid with semi-axis of 80 mgal length of 500 Km, and 300 Km, whose volume gives for (34)

$$M \simeq 6 \times 10^{20} \text{ grams} \qquad (35)$$

The anomalous mass is given by $\Delta\rho$ Vol., and letting $\Delta\rho = -0.6$, say at worst, the anomalous volume is

$$\text{Vol.} \simeq 10^{21} \text{ cm}^3 ;$$

or

$$\text{Vol.} = 10^{6} \text{ Km}^3 .$$

This result based on only the gravity anomaly is surprisingly similar to the magnetic estimate given already (eq. 25).

Effective Density Contrast:

The broad nature of the anomaly relative to its source suggests an anomaly model in the form of a pile of disks. The actual computation shows clearly, however, the attraction to be nearly identical to the Bouguer attraction of an infinite slab. The attraction of laterally infinite slab of anomalous density $\Delta\rho$ and thickness h is

$$\Delta g_B = 2\pi \Delta\rho \, Gh, \tag{37}$$

where G is the universal gravitational constant (6.67×10^{-8} cm^3 g^{-1} s^{-2}). The observed anomaly is about -80 m Gals relative to the surrounding region, hence the density contrast is

$$\Delta\rho = \Delta g_B / 2\pi Gh \tag{38}$$

or

$$\Delta\rho = \frac{-1.91}{h} \tag{39}$$

where h is now given in kilometers. The effective source thickness surely lies in the range 5 - 40 Km and then the density contrast lies in the range

$$-.5 \leq \Delta\rho \leq -.05, \tag{40}$$

and $-.2$ g cm^{-3} might be a fair estimate of the effective density contrast.

Conclusions

The anomaly-causing body probably lies at a depth of about 25 - 70 Km with an apparent susceptibility contrast of .01 - .02 (cgs), a dipole moment of about 3.5×10^{18}, a volume of about 10^6 Km^3, and an effective density contrast of -.05 to -.5 g cm^{-3}. The volume satisfies both magnetic and gravity constraints. This apparent susceptibility contrast is atypical of normally-encountered rocks.

Anomaly Source Characteristics

Parameter			Method and Assumptions
Volume	=	7×10^5 Km^3	dipole moment and suscept. est.
	=	10^6 Km^3	Gauss's Theorem and gravity anomaly
Depth	=	< 70 Km	induced mag., sphere
	=	26 Km	vertical derivative of mag. anomaly
Suscept. contrast	=	> .0126	induced mag., sphere at depth = radius
	=	> .0238	hor. dipole, depth = ½ length
dipole moment	=	3.6×10^{18}	(c.g.s), horizontal dipole
mass deficiency	=	6×10^{20} g	Gauss's Theorem
density contrast	=	-.05 to -.5	Bouguer effect (g cm^{-3})

Cause of the Anomaly

The close spatial correlation between the Bouguer gravitational field, the magnetic anomaly, and the large Oubangui sedimentary basin suggests the csuse of these anomalous fields is associated with basin development. The sedimentary basin is the surface manifestation of a deeper, large-scale orogenic development. A dense basic intrusion rising from the mantle and penetrating the lower crust, eventually stopping due to loss of buoyancy, and then upon cooling sinking slightly again would be reflected at the surface by formation of a sedimentary basin. More quantitatively, the hot intrusion will rise into the crust until its hydrostatic head or buoyancy is lost, it will then cool and become denser and sink some distance until it encounters a wall rock density similar to itself. The sinking distance can be roughly estimated by assuming an increase in crustal density with depth which obeys $d\rho/dz = x$, say, where ρ is density, z is depth (Km) and x is some constant, x is probably of the order .5/40 to .3/40. The intrustion in cooling by about 1000°C undergoes a density increase of about $\Delta\rho \approx \rho - \rho(1-\alpha\Delta T)$, where ρ is the initial intrusive density at its highest point in the crust, α is the coefficient of thermal expansion, and ΔT is the change in temperature upon cooling. For $\rho = \sim 3.00$ g cm^{-3}, $\alpha = 3 \times 10^{-5}$ deg^{-1}, and $\Delta T = -1000$ deg,

$$\Delta\rho = \rho - \rho\,(1-\alpha\Delta T) = -.09 \qquad (41)$$

and by using the previous relation for density variation in the crust

$$\frac{d\rho}{x} = \Delta z \sim \frac{\Delta\rho}{x} = \Delta z \qquad (42)$$

the sinking distance is

$$-\Delta z \sim 8 - 13 \text{ Km} \qquad (43)$$

depending on the exact choice of x. This result completely ignores the effect of the root of the sinking intrusion being increasingly supported by the underlying denser mantle during cooling and isostatic adjustment; it is an upper bound.

The sinking of the intrusive will cause the crust to be warped downward regardless of whether it behaves elastically or viscously. The elastic case is easily modeled by loading a thin plate which for the large mass involved here is suffiecient to cause a deflection of at least several kilometers (e.g. Heiskanen and Vening Meinesz, 1958, p. 346). The viscous case is less clear perhaps but it can be easily seen by considering the stream lines about a moving body, say a sphere, sinking in a still fluid. Below the body the fluid is bunched up or pushed outward and above the body it is drawn down. During draw-down of the surface a basin forms catching sediments. The sinking distance (43) is an upper bound on the basin depth; more probably the basin is only a fraction of this estimate (i.e. 4 - 10 km).

The density of the basin sediments will be somewhat less than that of the surrounding crustal rock from which they were derived. This density difference is probably no greater than 0.1 g cm^{-3}. The Bouguer attraction due to 7 Km of sediments with $\Delta\rho = -0.1$ is about -30 mgls. Substrating this from the main anomaly we are left with a gravity anomaly of about -50 mgls to explain. From (39) an effective source density contrast is -1.2/h, where h is the source thickness, assuming an infinite slab model. If the crust, inclusive of the intrusion, were of uniform density, the negative Bouguer anomaly corrected for the sedimentary basin would arise solely from the root of the intrusive protruding into the mantle. The root need not be very thick, for if the intrusion is of basic or ultra-basic composition, which is quite likely, its density contrast may be about -0.2 g cm^{-3}, whence a 6 Km thick slab will produce a -50 mgl anomaly. If the part of the intrusive within the crust is denser than the average crust - it is certainly not lighter since it would not have sunk to form the basin - the root thickness must be even greater. There is little sign, however, that an extensive root exists below the basin. The area should be close to isostatic equilibrium, yet the low elevation($\sim$ 450 m) and flat topography ($\pm \sim$ 100 m) clearly reflects no great Moho topography either. Thus most of the intrusive probably lies within the lower crust with a subordinate part acting as a root within the mantle; the crustal intrusive mass is probably slightly denser than the crust. Since the overall gravity anomaly is negative and the crustal intrusive probably produces a small positive anomaly the root and/or the basin must either be thicker or less dense than previously estimated. If the intrusive mass is roughly in isostatic equilibrium than the ratio of the

thickness of the crustal intrusive (h_c) to the mantle root (h_m) is given by

$$\frac{h_c}{h_m} \simeq \frac{-\Delta\rho_m}{\Delta\rho_c} \qquad (44)$$

where $\Delta\rho_m$ and $\Delta\rho_c$ are, respectively, the intrusive density contrast with the mantle and the crust. For the probable values of $\Delta\rho_m \simeq -0.25$ to .35 and $\Delta\rho_c \simeq .05$, $h_c \sim 5 - 7h_m$.

The following model approximately matches the observed gravity anomaly. Consider three circular disks portraying the sedimentary basin, the crustal intrusive, and the root with thicknesses of, respectively, 10, 25, and 10 km, the top of each disk lies, respectively, at 0, 15, and 40 km below the surface and have the same radius of 225 km; the density contrasts are -.15, 0.1, -.25 g cm^{-3}, respectively. The anomaly caused by this simplistic model is about -75 mgls. The lateral extent of the upper and lower disk is insensitive to the model, only the extent of the middle, lower crustal, disk is significant in the calculation. This rude model satisfies isostatic, mass, and geological constraints.

The absolute density of the intrusion is probably about 3.00 near its top and about 3.15 near its bottom. If so, it is probably gabbroic to ultra-basic in composition; its highly magnetic character is consistent with this identification. This basic intrusion has the qualities of a large diapir which having risen out of the mantle has become encumbered in the lower crust. Its gross structure is probably much like a lacolith with a mushroom-shaped head and a thin tail extending more deeply into the mantle; this is speculation.

The abrupt truncation of the magnetic but not the gravity anomaly near Grimari may indicate the upper intrusion morphology to be controlled by some local crustal structure. The appearance of magmatites near Grimari may indicate local shallowing of the basin and the absence of extensive intrusive at depth.

A possible difficulty with this model may arise if the broadly basaltic intrusive is in the eclogite metamorphic facies near the base of the crust. Eclogite is the high pressure equivalent of basalt. If so, the magnetite will break down to form rutile and an iron component in garnet (see e.g. Ringwood, 1975) rendering the eclogite nonferromagnetic. This transition is univariant with pressure and temperature and at any temperature it takes place over a pressure range of about 15 kb or about 40 km. The geotherms estimated for the C.A.E. (Figure 6) suggest the base of the intrusive here may be in the midst of this transition, hence it is likely that the rock is ferromagnetic.

Surficial Geological Evidence

The lower metamorphic rocks of the Oubangui Basin, especially those cropping out in the western part of the basin, commonly contain metabasalts. These basic lavas may be the surface expression of the intrusion. A less direct expression of the intrusive may be the undiscovered kimberlite pipes which surely exist in this region. Diamondiferous gravels exist in some abundance on the lateral boundaries of the Oubangui Basin. Heavy minerals separated from these gravels show very magnesian olivine ($\sim Fo_{92}$), orthopyroxene ($\sim En_{85}$); and pyrope-rich garnet which are characteristic of kimberlite pipes. These pipes which have vented at the earth's surface could be related to the massive intrusion lying deeper within the crust.

Meteoritic Source

Green (1975) has suggested a buried meteorite as a source for the magnetic anomaly. Although such a source may create a sufficiently large magnetic anomaly, its large negative buoyancy would cause it to slowly sink towards the core. The anomalous mass determined from the Bougner gravity field indicates not a mass excess but a mass deficiency associated with the magnetic anomaly. This seems unlikely if a meteorite were the source. Nevertheless if the volume associated with the magnetic anomaly is given a meteorite density and this negative buoyancy is equated to the shear stress on its edges, assuming it to be a sphere, its descent velocity is

$$V = \frac{\Delta M g}{G \pi a \mu} \qquad (45)$$

For $\Delta M \sim 10^{21}$, $g = 10^{3}$ cm s^{-2}, $\underline{a}$ which is the body radius of 10^{7} cm, and the crustal viscosity, $\mu = 10^{24}$ g cm^{-1} s^{-1}, the body would sink at about 5×10^{-9} cm s^{-1}. In the course of one billion years (3×10^{16} s) it would sink more than 1,000 km and would now be wholly within the core. A meteorite is considered an unlikely source of the magnetic anomaly.

References

Bichan, R., 1970, The evolution and structural setting of the Great Dyke, Rodesia, in African magmatism and tectonics, Clifford and Gass, (eds.), Hafner Pub. Co. Darien, Conn. 461 p.

Cahen, L., 1954, Geologie du Congo Belge, H. Vaillant-Cormanne, S. A., Liege, 577 p.

Cahen, L., and N. J. Snolling, 1966. The geochronology of equatorial Africa, North-Holland Pub. Co., Amsterdam, 195 p.

Carmichael, I. S. E., 1964, The petrology of Thingmuli, a tertiary volcano in eastern Iceland, J. Petrology, 5, p. 435-460.

Chapman, D. S. and H. N. Pollack, 1975, Global heat flow: a new look, Earth Planet. Sci. Letters, 28, p. 23-32.

Clifford, T. N., 1966, Tectono-metallogenic units and metallogenic provinces of Africa, Earth and Planet. Sci. Lets, 1, 421.

Clifford, T. N., 1970, The structural framework of Africa, in African magmatism and tectonics, Clifford and Gass (eds.), Hafner Pub. Co. Darien, Conn. 461 p.

Clifford, T. N., 1971, Location of mineral deposits, in understanding the earth, Gass, Smith and Wilson (eds.), M. I. T. Press, Cambridge, Mass., 383 p.

Cummings, D. and G. I. Shiller, 1971, Isopach map of the earth's crust, Earth-Sci. Rev., 7, p. 97-125.

Dobrin, M. B., 1976, Introduction to geophysical prospecting, McGraw-Hill Book Co., 630 p.

Furon, R., 1963, Geology of Africa, Hafner Pub. Co., New York, 377 p.

Gass, I. G., D. S. Chapman, H. N. Pollack and R. S. Thorpe, 1977, Geological and geophysical parameters of mid-plate volcanism, Phil. Trans. Roy. Soc. London.(in the press).

Gerard, J., and G. Gerard, 1954, Succession et eassi de correlation des terrains du soubassement en A. E. F. C. R. Reun. Ass. Serv. Geol. Afr., Nairobi, p. 117.

Gerard, G., and J. Gerard, 1952, Stratigraphie du Precambrien de l'Oubangui-Chari occidental. Bull. Geol. Soc. Fr. 6^{e} ser. ii, p. 467.

Gerard, G. 1958, Caste geologique de l'Afrique Equitoriale Francaise au 1/2,000,000. Notice Explicative. Dr. Mines Geol. A. E. F. (with full bibliography)

Godivier, R. and L. LeDonche, 1956, Reseau magnetique reme au lei Janiver 1956: Republique centra africaine Tchad Meridional, ORSTOM, 19 p.

Goldich, S. S., 1973, Ages of Precambrian banded iron formations, Economic Geology, 68, p. 1126-1134.

Grant, F. S., and G. F. West, 1965, Interpretation theory in applied geophysics, McGraw-Hill Book Co., New York, 583 p.

Green, A. G., 1975, Interpretation of Project MAGNET aeromagnetic profiles across Africa, Geophys. Jour. Roy. Astronom. Society.

Haughton, S. H., 1963, The stratigraphic history of Africa south of the Sahara, Oliver and Boyd, London, 365 p.

Heiskanen, W. A., and F. A. Vening Meinesz, 1958, The earth and its gravity field, McGraw-Hill Book Co., New York, 470 p.

Holmes, A. A., 1965, Principles of physical geology, (2nd ed), The Ronald Press Co., New York, 1288 p.

James, H. L., 1955, Zones of regional metamorphism in the Precambrian of northern Michigan, Bull. Geol. Soc. Amer. 66, p. 1455-1488.

Labrousse, B., 1972, Essai de synthese sure la R. C. A., unpublished report, 76 p.

Marsh, B. D. and J. G. Marsh, 1976, On global gravity anomalies and two-scale mantle convection, Jour. Geophys. Research, 81, p. 5267-5280.

Mestraud, J. L., 1953, Carte geologique de reconnaissance au 500,000 eme. Feuille Bangassou-Ouest, avec Notice Explicative Dir. Mines. Geol. A. E. F.

Nettleton, L. L., 1976, Gravity and magnetics in oil prospecting, McGraw-Hill Book Co., 464 p.

Pollack, H. N., and D. S. Chapman, 1977, Mantle heat flow, Earth Planet. Sci. Letters (in the press).

Pouit, G., 1959, Etude geologique des formations metamorphiques, granitiques et charnokitiques de la region de Fort Crampel, Bull. de la Direction des Mines et de la Geologie, Gouvernement General de l'Afrique Equatorial Francaise, 143 p.

Regan, R. D., 1976, The Bangui magnetic anomaly, Central African Republic, Final Trip report, Project Report (IR) CAR-1, 25 p.

Regan, R. D., J. C. Cain, and W. M. Davis, 1975, A global magnetic anomaly map; Jour. Geophys. Research, 80, p. 794.

Regan, R. D., W. M. Davis, and J. C. Cain, 1973, The Bangui magnetic anomaly (abs.); Trans. Amer. Geophys. Union, 54, p. 236.

Ringwood, A. E., 1975, Composition and petrology of the earth's mantle, McGraw-Hill Book Co., New York, 618.

Roy, F. F., D. D., Blackwell, and E. R. Decker, 1972, Continental heat flow, in the nature of the solid earth, E. C. Robertson, J. F. Hays, and L. Knopoff (eds.), McGraw-Hill Book Co., New York, 677 p.

Sims, P. K., 1976, Precambrian tectonics and mineral deposits, Lake Superior Region, Economic Geology, 71, p. 1092-1127.

Stanton, R., 1972, Ore Petrology, McGraw-Hill Book, Co., New York.

Stockard, H. P., 1971, Worldwide surveys by Project MAGNET, World magnetic survey, 1957-1969: International Assoc. Geomag. Aeron. Bull. 28, p. 60-64.

Eratta

The word charnockite has been misspelled throughout.